

Quantum Features of the Thermal Two-Qubit Quantum Rabi Model in Ultra- and Deep-Strong Regimes

Ciro Micheletti Diniz ^{1,*} Gabriella G. Damas ² Norton G. de Almeida ² Celso J. Villas Bôas ¹ and G. D. de Moraes Neto ^{3,†}

¹*Departamento de Física, Universidade Federal de São Carlos, Rodovia Washington Luís, km 235 - SP-310, 13565-905 São Carlos, SP, Brazil*

²*Instituto de Física, Universidade Federal de Goiás, 74.001-970, Goiânia - GO, Brazil*

³*College of Physics and Engineering, Qufu Normal University, Qufu, 273165, China*

Quantum correlations and nonclassical states are indispensable resources for advancing quantum technologies, and their resilience at finite temperatures is crucial for practical experimental implementations. The two-qubit quantum Rabi model (2QQRM), a natural extension of the quantum Rabi model, describes two qubits coupled to a single bosonic mode and has been extensively studied in cavity quantum electrodynamics, superconducting circuits, and quantum information science. In this work, we investigate the persistence of quantum correlations and nonclassical states in the 2QQRM at thermal equilibrium, focusing on the ultrastrong and deep strong coupling regimes. Through a systematic analysis of quantumness quantifiers, we demonstrate the emergence of long-lived quantum correlations, even in the presence of thermal noise. Notably, we uncover striking phenomena arising from the interplay between detuning and deep strong-coupling: in the high-frequency limit, where the qubit energy exceeds the cavity-mode energy, quantum criticality emerges, leading to a high degree of photon squeezing. In contrast, the opposite regime is characterized by robust qubit-qubit quantum correlations. Importantly, we show that both dispersive regimes exhibit quantum features that are remarkably robust to parameter fluctuations, making them advantageous for maintaining quantum coherence. These results highlight the exceptional resilience of quantum resources in the 2QQRM and provide valuable insights for developing quantum technologies operating under realistic, finite-temperature conditions.

I. INTRODUCTION

The concept of quantumness, or nonclassicality, refers to the unique traits of quantum systems that cannot be fully explained by classical theories, whether deterministic or probabilistic. These traits include phenomena such as entanglement, coherence, and superposition, all of which challenge classical interpretations of reality. Quantum correlations in nonclassical states have become a foundational aspect of modern quantum information theory [1, 2], with far-reaching implications for both theoretical research and the development of practical quantum technologies [3, 4]. These correlations enable quantum information tasks such as secure communication [5, 6], quantum sensing [7–13], and quantum simulation [14]. At the same time, understanding the dynamics of quantum systems is crucial for the advancement of quantum technologies, where the effects of decoherence [15] and the transition from quantum to classical [16] remain significant challenges. Techniques such as decoherence-free subspaces [17–19], dynamical decoupling [20, 21], and reservoir engineering [22–25] have been proposed to mitigate these challenges and extend the lifetimes of nonclassical states.

Among the various platforms for generating and manipulating nonclassical states, quantum systems with

light-matter interactions stand out as key candidates [26, 27]. Recent advances in the ultrastrong-coupling (USC) [28–30] and deep strong-coupling (DSC) [31, 32] regimes have enabled the exploration of nonclassical behaviors even in the ground state of light-matter systems. In contrast to the strong-coupling (SC) regime [33–37], where the coupling strength is comparable to or larger than the system decay rates but extremely small compared to system frequencies, the USC and DSC regimes exhibit a rich array of phenomena, including squeezing, entanglement, and photon antibunching [38–41]. These effects arise due to the increased coupling strength, which becomes comparable to the system frequencies, allowing for more pronounced quantum correlations.

The quantum Rabi model (QRM), describing the interaction between a two-level atom (qubit) and a single-mode cavity field, serves as the fundamental framework for studying light-matter interactions [42–45]. This model has been widely studied across various fields, such as quantum optics [46], entanglement generation [47], quantum thermodynamics [48–52], and the study of quantum phase transitions (QPTs) [53–58]. Modifications to the QRM, such as the anisotropic quantum Rabi model (AQRM) [59, 60] and the Jaynes-Cummings model (JCM) [61], provide even richer dynamics by incorporating different coupling terms and interactions. Both the AQRM and the JCM are known to exhibit first-order quantum phase transitions, which influence quantum thermalization and the persistence of quantum correlations at thermal equilibrium [62–65].

This work builds upon the two-qubit quantum Rabi

* ciromd@outlook.com.br

† gdmneto@gmail.com

model (2QQRm) [66–69] and explores persisting quantum effects in light-matter systems operating in the USC and DSC regimes at thermal equilibrium. This model has been investigated in cavity quantum electrodynamics (QED) [70], superconducting circuit QED [71–73], quantum information science [74], and cold atom physics [75]. Applications range from preparing entangled atomic states in cavity QED [76, 77] to realizing two-qubit logic gates and enabling coherent storage and transmission in quantum information systems [78–80]. The 2QQRm has been analyzed using several methods, including exact approaches such as Bargmann-space techniques [67, 81] and various approximations like the adiabatic method [69], perturbation theory [66], the extended coherent state method [82], the zeroth-order approximation [69], and the generalized rotating-wave approximation (GRWA) [83].

Regarding the previous techniques, the zeroth-order approximation is applicable when the qubit transition frequency Δ is much smaller than the field frequency ω , even in the ultrastrong coupling regime. Additionally, in contrast to the rotating-wave approximation (RWA) that neglects counter-rotating terms and is valid to small couplings $g \ll \omega$ and detunings following $|\omega - \Delta| \ll |\omega + \Delta|$, the GRWA extends to negative detunings ($\delta = \omega - \Delta < 0$) and ultrastrong coupling ($g < \omega$) [83]. These techniques have been employed to determine the energy spectrum, dynamics, and entanglement evolution of the system. Notably, for the 2QQRm, there exists a special dark state with at most one photon and constant eigenenergy [84], where two identical qubits form a spin singlet, and the eigenstates are just products of these singlets and a Fock state. This dark state enables the deterministic fast generation of W states [85] and high-quality single-photon sources [86] via adiabatic evolution. Recently, thermally-induced coherences in the 2QQRm have been investigated [87]. Additionally, new extensions of the model have been explored, including a two-qubit Rabi model incorporating explicit spin-spin interactions [88] and a tripartite quantum Rabi model, where a single bosonic mode couples to two (1/2)-spin particles via a spin-spin interaction, resulting in spin-spin-boson coupling [89].

A central question arises in the context of the 2QQRm: can long-lived, highly correlated nonclassical states persist even in the presence of a thermal reservoir? This issue is crucial for the development of current experimental platforms where maintaining quantum coherence at finite temperatures is a significant challenge.

In this work, we address the aforementioned question by analyzing the *quantumness* of the global system steady state and deepen our studies in the finite temperature-coupling strength phase diagram considering broader ranges of parameters. To this end, the paper is structured as follows: In Sec. II, we present the model and revisit some well-known results for the closed system scenario. In Sec. III, we define the nonclassicality measures and witnesses used throughout our analy-

sis. In Sec. IV, we present our findings, focusing on the temperature-dependent behavior of the system. Finally, Sec. V contains our concluding remarks.

II. THE MODEL

The Hamiltonian of the two-qubit quantum Rabi model (2QQRm), as illustrated in Fig. 1(a), is given by ($\hbar = 1$) [66, 67]:

$$\hat{H} = \omega \hat{a}^\dagger \hat{a} + \sum_{i=1}^2 \frac{\Delta_i}{2} \hat{\sigma}_z^{(i)} + \sum_{i=1}^2 g_i (\hat{a} + \hat{a}^\dagger) (\hat{\sigma}^{(i)+} + \hat{\sigma}^{(i)-}), \quad (1)$$

where the quantum system consists of two qubits (represented by the Pauli matrices $\hat{\sigma}_x, \hat{\sigma}_y, \hat{\sigma}_z, \hat{\sigma}^\pm$) interacting with a single-mode bosonic field. In this model, \hat{a} and \hat{a}^\dagger are the boson annihilation and creation operators with frequency ω . The coupling strength g_i describes the interaction between the i -th qubit and the bosonic field, while the transition frequencies of the two qubits are, respectively, Δ_1 and Δ_2 .

One distinctive feature of the 2QQRm is its parity symmetry \mathbb{Z}_2 , akin to the standard quantum Rabi model [30]. This symmetry can be identified by examining the total excitation number operator $\hat{n} = \hat{a}^\dagger \hat{a} + \hat{\sigma}^{(1)+} \hat{\sigma}^{(1)-} + \hat{\sigma}^{(2)+} \hat{\sigma}^{(2)-}$ and the parity operator $\hat{\pi} = \exp(i\pi \hat{n})$. The 2QQRm satisfies the commutation relations $[\hat{H}, \hat{n}] \neq 0$ and $[\hat{H}, \hat{\pi}] = 0$. As a result, two important consequences follow: (i) the expected number of excitations in both the qubits and the bosonic mode is non-zero, even in the ground state, and (ii) $\hat{\pi}$ has eigenvalues $\langle \hat{\pi} \rangle = \pm 1$, depending on whether the total excitation number is even or odd. The Hilbert space can be naturally divided into triplet and singlet sectors. The triplet sector consists of the states $\{|\Phi_{\pm, n}\rangle, |\Psi_{+, n}\rangle\}$, while the singlet sector contains the states $\{|\Psi_{-, n}\rangle\}$. The states in these sectors are defined as:

$$|\Phi_{\pm, n}\rangle = \frac{1}{\sqrt{2}} |n\rangle (|g, g\rangle \pm |e, e\rangle); \quad (2)$$

$$|\Psi_{\pm, n}\rangle = \frac{1}{\sqrt{2}} |n\rangle (|g, e\rangle \pm |e, g\rangle), \quad (3)$$

where $|n\rangle$ is the Fock state of n photons, and $|g\rangle$ ($|e\rangle$) is the ground (excited) state of the qubits.

In the singlet sector, the eigenstates with an odd photon number n belong to the positive parity subspace, while those with an even photon number n belong to the negative parity subspace. This symmetry allows the analytical solution of the 2QQRm using methods such as the Bargmann-Fock space [67, 81] of analytic functions and the Bogoliubov operator approach [90], which are also used for the standard QRm.

To study the quantum correlations and quantum nonclassicality in the 2QQRm, we aim to examine the system at thermal equilibrium. In this context, the system interacts with a reservoir at temperature \mathbf{T} , and we

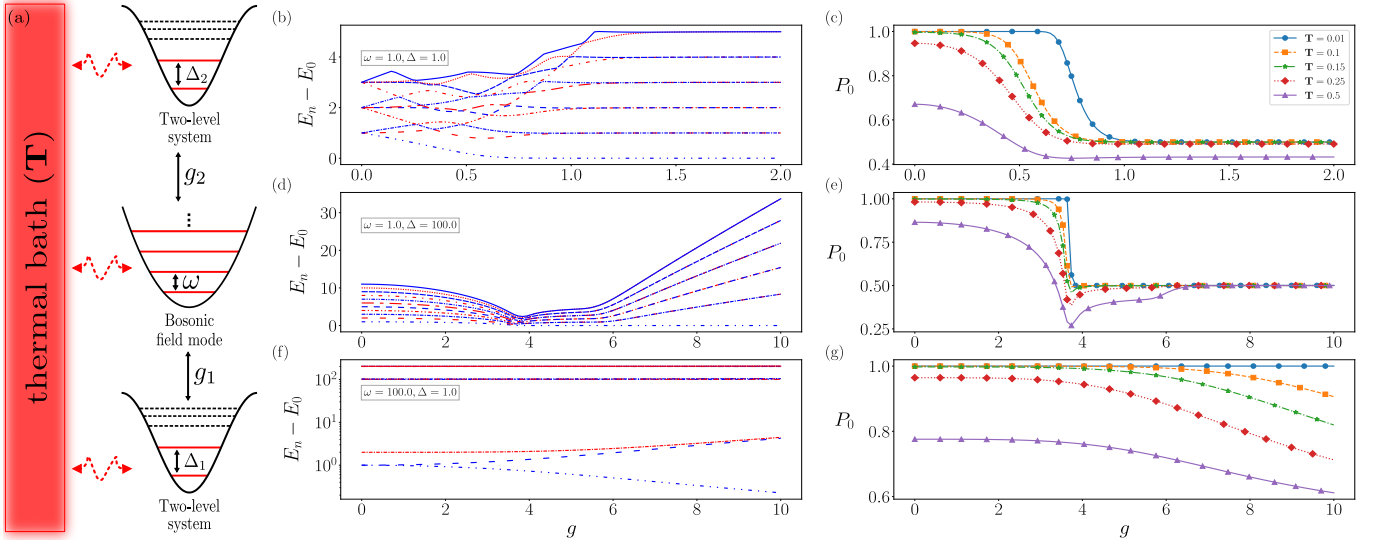


FIG. 1. Nonclassical effects in thermal Two-Qubit Quantum Rabi Model. Panel (a) illustrates the model studied in this work. A bosonic field mode of frequency ω interacts with two atoms, modeled as two-level systems. The i -th atom couples to the field mode with strength g_i and has a transition frequency Δ_i . All components are in thermal equilibrium with a shared bath at temperature \mathbf{T} . Additionally, we present the energy difference $E_n - E_0$ between the n -th excited state (in increasing order, starting with $n = 1$) and the ground state considering the total system, along with the equilibrium Gibbs ground-state population P_0 , as functions of the qubit-field coupling strength g for degenerate qubits. We present three different interaction regimes: panels (b) and (c) represent the resonant case with $\omega = \Delta = 1.0$, panels (d) and (e) depict the high-frequency qubit regime where $\Delta = 100.0$, $\omega = 1.0$, and, finally, panels (f) and (g) correspond to the adiabatic quantum oscillator regime with $\omega = 100.0$, $\Delta = 1.0$. In the energy plots, states with different parities are distinguished using blue and red lines. Still, the population distributions are computed for a range of temperatures, with all quantities expressed in units of ω in panels (b)–(e) and in units of Δ in panels (f) and (g).

seek to obtain the steady state of the system under these conditions. To ensure the steady state represents the true quantum state at thermal equilibrium for an arbitrary set of coupling strengths, one must adopt a Born-Markov master equation in a dressed picture [65, 91]. In the dressed-state picture, quantum jumps occur between the eigenstates of the full Hamiltonian, which accounts for both the system and its interaction with the reservoir. This contrasts with the standard master equation approach, where jumps are determined solely by the system's free energy.

By considering conditions that lead to thermal equilibrium—such as when the qubits and the mode share the same temperature, $T_{\text{mode}} = T_{\text{qubits}} = \mathbf{T}$, or when only a single subsystem is coupled to the reservoir—the system's dynamics can be effectively described using the dressed master equation. The dissipative evolution is governed by

$$\frac{d}{dt}\hat{\rho} = -i[\hat{H}, \hat{\rho}] + \sum_{\substack{u=a, \sigma^{(i)} \\ k < j}} \{\Gamma_u^{jk} n_u(\Delta_{jk}) \mathfrak{D}[|\phi_j\rangle\langle\phi_k|, \hat{\rho}] \\ + \Gamma_u^{jk} [1 + n_u(\Delta_{jk})] \mathfrak{D}[|\phi_k\rangle\langle\phi_j|, \hat{\rho}]\} = \mathcal{L}(t)\hat{\rho}, \quad (4)$$

where $n_u(\Delta_{jk})$ is the number of thermal photons of the u -th bath associated with the energy gap $\Delta_{jk} = E_j - E_k$, $|\phi_k\rangle$ and E_k are, respectively, the eigenstates

and eigenenergies of the full Hamiltonian \hat{H} , satisfying $\hat{H}|\phi_k\rangle = E_k|\phi_k\rangle$, and $\mathcal{L}(t)$ is the Liouvillian superoperator, with the Lindblad dissipator given by

$$\mathfrak{D}[\hat{O}, \hat{\rho}] = \frac{1}{2}[2\hat{O}\hat{\rho}\hat{O}^\dagger - \hat{\rho}\hat{O}^\dagger\hat{O} - \hat{O}^\dagger\hat{O}\hat{\rho}]. \quad (5)$$

In Eq. (4), we also define the dissipation rates

$$\Gamma_u^{jk} = \gamma_u(\Delta_{jk}) |S_u^{jk}|^2, \quad (6)$$

which consist of two distinct contributions. The first is the spectral function,

$$\gamma_u(\Delta_{jk}) = 2\pi \sum_k |\lambda_{k,u}|^2 \delta(\Delta_{jk} - \omega_k), \quad (7)$$

where $\lambda_{k,u}$ accounts for the u -th thermal bath coupled to a single-mode boson field with the frequency ω_k . The second contribution comes from the transition coefficients of the i -th qubit (q) and the cavity mode (c), respectively, given by

$$S_{q^{(i)}}^{jk} = \langle\phi_j|(\hat{\sigma}^{(i)+} + \hat{\sigma}^{(i)-})|\phi_k\rangle, \quad (8)$$

$$S_c^{jk} = \langle\phi_j|(\hat{a}^\dagger + \hat{a})|\phi_k\rangle. \quad (9)$$

To satisfy the necessary conditions for the validity of the master equation presented in Eq. (4), we consider the

Ohmic case:

$$\gamma_u(\Delta_{jk}) = \pi\alpha\Delta_{jk}e^{-|\Delta_{jk}|/\omega_c}, \quad (10)$$

where α is the coupling strength between the system and the environment and ω_c is the cutoff frequency of thermal baths. Throughout all numerical simulations performed, we consider $\alpha = 0.001\omega$ and $\omega_c = 10\omega$. We note that for Gibbs states of the reservoir at temperature \mathbf{T} , the correlation functions also obey the Kubo-Martin-Schwinger (KMS) relations [91], i.e., $\gamma_u(-\Delta_{jk}) = \gamma_u(\Delta_{jk})e^{-\Delta_{jk}/k_B\mathbf{T}}$, where k_B is the Boltzmann constant. Under these equilibrium conditions, the system reaches a steady state described by the canonical ensemble, with a density matrix ($k_B = 1$)

$$\hat{\rho}_{\text{ss}} = \sum_k \frac{e^{-E_k/\mathbf{T}}}{\mathcal{Z}} |\phi_k\rangle\langle\phi_k|, \quad (11)$$

where $\mathcal{Z} = \sum_k e^{-E_k/\mathbf{T}}$ is the partition function. The steady-state populations are then given by

$$P_k = \frac{e^{-E_k/\mathbf{T}}}{\mathcal{Z}}, \quad (12)$$

where the partition function \mathcal{Z} guarantees that the total population sums to one, ensuring the proper statistical normalization.

To enhance the clarity of the numerical results, we follow by providing a concise review of significant limit regimes of our model.

Starting by the dispersive limit, where the qubits are far detuned from the resonator compared to the coupling strength, we have the condition $g\sqrt{n+1} \ll |\Delta - \omega| \ll |\Delta + \omega|$, where $n = \langle \hat{a}^\dagger \hat{a} \rangle$ is the number of photons in the resonator. The first inequality indicates the dispersive regime, where the coupling g is small relative to the detuning, while the second condition is typically used to derive the rotating wave approximation Hamiltonian. Beyond the RWA, the detuning does not need to be smaller than both Δ and ω , as long as $g \ll |\Delta - \omega| = \delta$ holds.

For two qubits, considering the RWA, the dispersive Hamiltonian is [92]

$$\begin{aligned} \hat{H}_{\text{disp}} &= \omega \hat{a}^\dagger \hat{a} + \frac{1}{2} \sum_{j=1}^2 \left(\Delta_j + \frac{g_j^2}{\delta_j} \right) \hat{\sigma}_z^{(j)} \\ &+ \sum_{j=1}^2 \frac{g_j^2}{\delta_j} \hat{a}^\dagger \hat{a} \hat{\sigma}_z^{(j)} + J_{12} \left(\hat{\sigma}_+^{(1)} \hat{\sigma}_-^{(2)} + \hat{\sigma}_-^{(1)} \hat{\sigma}_+^{(2)} \right), \end{aligned} \quad (13)$$

where J_{12} is the effective coupling between the two qubits, given by

$$J_{12} = g_1 g_2 \left(\frac{1}{\delta_1} + \frac{1}{\delta_2} \right), \quad (14)$$

with $\delta_i = \Delta - \omega_i$ being the detuning between the i -th qubit and the field mode.

When extending this Hamiltonian beyond the RWA, we obtain

$$\begin{aligned} \hat{H}_{\text{disp}} &= \hbar\omega \hat{a}^\dagger \hat{a} + \frac{1}{2} \sum_{j=1}^2 \Delta_j \hat{\sigma}_z^{(j)} + \bar{J}_{12} \hat{\sigma}_x^{(1)} \hat{\sigma}_x^{(2)} \\ &+ \sum_{j=1}^2 g_j^2 \left(\frac{1}{\delta_j} - \frac{1}{\Delta_j - \delta_j} \right) (\hat{a}^\dagger + \hat{a})^2 \hat{\sigma}_z^{(j)}, \end{aligned} \quad (15)$$

where the modified coupling strength is

$$\bar{J}_{12} = g_1 g_2 \left(\frac{1}{\delta_1} + \frac{1}{\delta_2} - \frac{1}{2\Delta_1 - \delta_1} - \frac{1}{2\Delta_2 - \delta_2} \right). \quad (16)$$

In the case of two qubits, the non-RWA treatment yields a qualitatively different effective model compared to the RWA. Specifically, the interaction between the qubits becomes of the Ising type ($\hat{\sigma}_x^{(1)} \hat{\sigma}_x^{(2)}$) in the non-RWA regime, while in the RWA, it corresponds to an XY-type interaction ($\hat{\sigma}_+^{(1)} \hat{\sigma}_-^{(2)} + \hat{\sigma}_-^{(1)} \hat{\sigma}_+^{(2)}$). In addition to this, the non-RWA Hamiltonian does not conserve the number of excitations, which has important implications for the design and implementation of two-qubit gates. More importantly, the coupling is no longer proportional to the photon number operator $\hat{a}^\dagger \hat{a}$, as in the RWA, but instead involves a parametric $(\hat{a}^\dagger + \hat{a})^2$ term. This modification opens the possibility for squeezing of the field, which can lead to nonclassical effects such as entanglement and photon-number squeezing, further complicating gate operations and providing richer dynamics for quantum information processing. For two degenerate qubits ($\Delta_1 = \Delta_2$) coupled to a single cavity, the ground state of the non-RWA Hamiltonian is $|0\rangle (|gg\rangle - \frac{J}{2\Delta} |ee\rangle)$, which exhibits qubit-qubit entanglement. In contrast, the corresponding ground state of the two-qubit RWA Hamiltonian is the product state $|0\rangle |gg\rangle$. These effective Hamiltonians shed light on the regime of coupling parameters where qubit-qubit quantum correlations arise.

In the deep strong coupling regime, where the coupling parameters $g_1, g_2 \gg \Delta_1, \Delta_2$, the two-qubit quantum Rabi model Eq. (1) can be approximated as a leading Hamiltonian [66] $\hat{H} = \hat{H}_0 + \hat{P}$, where \hat{H}_0 is diagonal and \hat{P} is the perturbation. When applying a general rotation $\hat{R}_y = e^{-i\frac{\pi}{4}\hat{\sigma}_y^{(1)}} \otimes e^{-i\frac{\pi}{4}\hat{\sigma}_y^{(2)}}$ that transform the qubit operators $\hat{\sigma}_x^{(j)}$ and $\hat{\sigma}_z^{(j)}$, the effective Hamiltonian becomes

$$\tilde{H}_0 = \omega \hat{n} + (\hat{a} + \hat{a}^\dagger) \left(g_1 \hat{\sigma}_z^{(1)} + g_2 \hat{\sigma}_z^{(2)} \right), \quad (17)$$

$$\tilde{P} = -\frac{1}{2} \left(\Delta_1 \hat{\sigma}_x^{(1)} + \Delta_2 \hat{\sigma}_x^{(2)} \right), \quad (18)$$

where the rotated Hamiltonian becomes diagonal,

$$\tilde{H}_0 = \hat{T}_D \left[\omega \hat{n} - \frac{1}{\omega} \begin{pmatrix} g_+^2 & 0 & 0 & 0 \\ 0 & g_-^2 & 0 & 0 \\ 0 & 0 & g_-^2 & 0 \\ 0 & 0 & 0 & g_+^2 \end{pmatrix} \right] \hat{T}_D^\dagger, \quad (19)$$

for a driven oscillator basis \hat{T}_D obeying

$$\hat{T}_D = \begin{pmatrix} \hat{D}(g_+/\omega) & 0 & 0 & 0 \\ 0 & \hat{D}(g_-/\omega) & 0 & 0 \\ 0 & 0 & \hat{D}(-g_-/\omega) & 0 \\ 0 & 0 & 0 & \hat{D}(-g_+/\omega) \end{pmatrix}, \quad (20)$$

with the displacement operator $\hat{D}(\alpha) = e^{\alpha\hat{a}^\dagger - \alpha^*\hat{a}}$ and $g_\pm = g_1 \pm g_2$.

Still, the approximated eigenvalues, including second-order corrections, exhibit a twofold degeneracy. The first-order correction due to the perturbation \tilde{P} is null, while the second-order correction arises from photon transitions mediated by the displacement operator, depending explicitly on the coupling strengths g_1 and g_2 . Once we are dealing with the DSC regime, where g_1, g_2 reach large values, these second-order corrections diminish, leading the spectral branches to converge toward the spectrum of a forced harmonic oscillator [66].

The next limit we consider is where the oscillator's characteristic frequency ω is large compared to the qubit's energy splitting (i.e., $\omega \gg \Delta_i$) and also large compared to the coupling strength ($\omega \gg g_i$). In this case, the oscillator can be considered to remain in its initial energy eigenstate (e.g., the ground state, first excited state, etc.), and this state evolves adiabatically in response to changes in the qubit's state.

It has been shown in Ref. [93] that in the regime $\Delta_i \leq 0.25\omega$, the adiabatic approximation holds, and the eigenstates of the system are product states of displaced Fock states for the photons and atomic states that are x -polarized, i.e., $|\Phi\rangle = |j, m\rangle|\phi_m\rangle$. Specifically, the qubits can be described using the simultaneous eigenstates of the operators $\hat{\sigma}_x^{(1)}$ and $\hat{\sigma}_x^{(2)}$, where $\hat{\sigma}_x^{(i)}|\pm\rangle = \pm 1|\pm\rangle$. In terms of these eigenstates, the states $|j, m\rangle$ of the collective spin operator $\hat{S}_x = \frac{1}{2}(\hat{\sigma}_x^{(1)} + \hat{\sigma}_x^{(2)})$ can be expressed as:

$$\begin{pmatrix} |1, 1\rangle \\ |1, 0\rangle \\ |0, 0\rangle \\ |1, -1\rangle \end{pmatrix} = \begin{pmatrix} 1 & 0 & 0 & 0 \\ 0 & \frac{1}{\sqrt{2}} & \frac{1}{\sqrt{2}} & 0 \\ 0 & \frac{1}{\sqrt{2}} & -\frac{1}{\sqrt{2}} & 0 \\ 0 & 0 & 0 & 1 \end{pmatrix} \begin{pmatrix} |+, +\rangle \\ |+, -\rangle \\ |-, +\rangle \\ |-, -\rangle \end{pmatrix}, \quad (21)$$

where $j \in \{0, 1\}$ and $m \in \{-1, 0, 1\}$. Additionally, $|\phi_m\rangle$ is the Fock state displaced by $\hat{D}(-mg)$.

The adiabatic approximation highlights a significant degree of quantum correlations between the qubits in this regime, in agreement with the effective Hamiltonian in Eq. (15), a conclusion that will be further substantiated by our forthcoming numerical results.

We now turn to the high-frequency limit, where the qubit adjusts adiabatically, i.e., $\Delta_i \gg \omega, g_i$. In this regime, quantum criticality emerges in QRMs and generalized QRMs [53–55], leading to abrupt changes at quantum phase transitions (QPT) due to quantum fluctuations. This phenomenon is exemplified by superradiance phase transitions (SPT), where excitations in the ground-state population occur [94]. Experimental ion trap stud-

ies [95] have confirmed second-order QPT in the QRM, with a rapid increase in both phonon numbers and ion excitations at the critical point. In the deep strong coupling regime, a zero-temperature photon vacuum instability drives the system toward a QPT at the critical coupling strength $g_c = \frac{\sqrt{\omega\Delta}}{2}$ [53–55]. Below g_c , the system resides in a normal phase, while it enters a superradiant phase above g_c . In the Dicke model [96, 97], the thermodynamic limit is attained as the number of particles increases. However, in few-atom systems, quantum phase transitions emerge in the classical oscillator limit, characterized by $\omega/\Delta \rightarrow 0$. A distinct thermodynamic limit arises in the two-qubit quantum Rabi model with spin-spin interactions [88], where criticality is determined by the infinite ratios of the spin-spin and spin-mode couplings to the mode frequency, independent of the spin-to-mode frequency ratios. Although this work does not primarily focus on the system's critical behavior, our findings in the $\Delta \gg \omega$ regime suggest its presence, as evidenced by the photon population and their pronounced nonclassicality.

We also briefly investigated the Liouvillian spectrum \mathcal{L} [98]. This analysis not only confirms the uniqueness of the equilibrium state described in Eq. (11), ruling out the possibility of a dissipative quantum phase transition, but also provides key insights into the system's relaxation timescale. Let $\{\mu_\alpha\}_{\alpha=0,1,2,\dots}$ denote the complex eigenvalues of \mathcal{L} , as defined in Eq. (4). In the parameter range analyzed in this work, numerical evaluation indicates that $\mu_0 = 0$ is non-degenerate, ensuring a unique and stable steady state. To quantify the relaxation timescale, we consider the Liouvillian gap [99], defined as the difference between zero (i.e., $\mu_0 = 0$) and the eigenvalue with the largest nonzero real part: $\mu_1 = -\max_{\alpha \neq 0} \text{Re}[\mu_\alpha]$. The Liouvillian gap determines the asymptotic decay rate and provides an estimate for the thermalization time, given by $t_{\text{th}} \approx |\mu_1|^{-1}$. To compare the relaxation time required to reach equilibrium in the 2QCRM, we calculate the ratio of the normalized Liouvillian gap $\mu_1(\omega, \Delta, g)$ to the gap of the decoupled system, $\mu_1(\omega, \Delta, g = 0)$. Our findings reveal: (i) near resonance ($\omega/\Delta \approx 1$), the ratio falls within the range $1/2 < \mu_1(\omega, \Delta, g)/\mu_1(\omega, \Delta, g = 0) < 2$; (ii) in the limit $\omega \gg \Delta$, the gap remains nearly unchanged, $\mu_1(\omega, \Delta, g)/\mu_1(\omega, \Delta, g = 0) \approx 1$; (iii) for $\Delta \gg \omega$, the ratio can vary significantly, spanning $1 < \mu_1(\omega, \Delta, g)/\mu_1(\omega, \Delta, g = 0) < 10^5$, with the upper bound corresponding to the extreme case of $\omega/\Delta = 10^{-3}$. These results are consistent with the thermalization time in the thermal ACRM [65] and with Ref. [100], which reported that the energy relaxation rate decreases as the system approaches criticality and may even vanish precisely at the critical point. Notably, a faster thermalization is essential for quantum thermodynamic applications, as shorter relaxation times can enhance the power of quantum heat engines. Additionally, thermalization dynamics play a key role in enabling the on-demand generation of equilibrium non-classical states for quantum information processing.

To conclude our review, we present in Fig. 1 the energy spectrum (with blue and red indicating different parity states) and steady-state population P_0 across different temperatures for degenerate qubits in various regimes. Figs. 1(b) and (c) show the resonant interaction regime ($\omega = \Delta$), where the energy levels exhibit significant anharmonicity, transitioning to a degenerate harmonic spectrum in the deep strong coupling limit. Figs. 1(d) and (e) illustrate the high-frequency qubit regime ($\Delta \gg \omega, g$), revealing distinct behaviors before and after the critical coupling $g_c = \frac{\sqrt{\omega\Delta}}{2}$. Figs. 1(f) and (g) show the adiabatic quantum oscillator regime ($\omega \gg \Delta, g$), where the system evolves adiabatically and the qubits track the oscillator's evolution in a nearly flat potential.

Lastly, numerical computations throughout this work were carried out using QuTiP [101], with a variable Fock basis employed to achieve convergence.

III. QUANTUM CORRELATION AND NONCLASSICALITY QUANTIFIERS

To investigate how the system's light-matter coupling influences thermal quantum correlations and thermal nonclassicality (i.e., quantum effects that persist even at thermal equilibrium) we focus on several key quantities that provide insights into these nonclassical properties. The quantifiers employed throughout this paper are designed to ensure a comprehensive description of the system, offering a multifaceted understanding of its quantum behavior. Specifically, we analyze:

1. **The zero-delay second-order correlation function, $G^{(2)}(0)$:** This quantifies photon bunching or anti-bunching, highlighting deviations from classical photon statistics. It reveals quantum characteristics by indicating whether photons tend to arrive together (bunching) or separately (anti-bunching) at the detector, thus serving as a tool for identifying single-photon sources.
2. **Bosonic field quadrature squeezing, ζ^2 :** This quantifies the squeezing of the electromagnetic field quadratures (such as position or momentum) below the vacuum state uncertainty limit whenever $\zeta^2 < 1$.
3. **Negativity, $\mathcal{N}(\hat{\rho})$:** This quantifies the degree of separability in a quantum state by examining the eigenvalues of the partial transpose of the density matrix. Here, it is employed to study entanglement between photons and qubits in the system.
4. **Mutual information, $\mathcal{I}(\hat{\rho})$:** This quantifies the total correlations, both classical and quantum, between subsystems in a quantum system, providing a complete measure of the shared information.

5. **Concurrence, $C(\hat{\rho})$:** This is an entanglement measure specific to two-qubit systems. It quantifies the extent to which a quantum state deviates from being separable. A concurrence value of zero indicates no entanglement between the two qubits.
6. **Quantum discord, $\mathcal{D}(\hat{\rho})$:** This captures the difference between total correlations (as measured by mutual information) and classical correlations that can be extracted via local measurements. It provides a nuanced view of quantum correlations beyond entanglement.
7. **Quantum coherence, C_{RE} :** This reflects the ability of a quantum system to exhibit interference effects, measuring the presence of superposition states through the nonzero off-diagonal elements of the density matrix.
8. **Local quantum uncertainty (LQU), $\mathcal{U}_A(\hat{\rho})$:** This quantifies the minimum uncertainty in local observables of a quantum system, offering insights into quantum features at the level of individual qubits.

In the following subsections, we provide detailed definitions and interpretations of each of these quantities, highlighting their significance in studying thermal nonclassicality and the impact of light-matter coupling.

A. Zero-delay second-order correlation function

Sub-Poissonian photon statistics serve as a signature of the quantum nature of light, distinguishing it from classical light descriptions. While this property does not always manifest in all quantum states [102, 103], its presence signals nonclassicality. The second-order correlation function $g^{(2)}(\tau)$ classifies light as follows: (i) $g^{(2)}(\tau) > 1$ for bunched light (classical chaotic), (ii) $g^{(2)}(\tau) = 1$ for coherent light (classical random), and (iii) $g^{(2)}(\tau) < 1$ for antibunched light (nonclassical) [102, 103].

In the USC regime, where strong light-matter interaction occurs, the zero-delay second-order correlation function is given by [104, 105]

$$G^{(2)}(0) = \frac{\langle (\hat{X}^-)^2 (\hat{X}^+)^2 \rangle}{\langle \hat{X}^- \hat{X}^+ \rangle^2}, \quad (22)$$

where $\hat{X}^+ = -i \sum_{k>j} \delta_{kj} X_{jk} |\phi_j\rangle \langle \phi_k|$ with $\hat{X}^- = (\hat{X}^+)^\dagger$, $\delta_{kj} = E_k - E_j$ being the energy gap, and $X_{jk} = \langle \phi_j | (\hat{a}^\dagger + \hat{a}) | \phi_k \rangle$. In the weak coupling limit, \hat{X}^+ reduces to $\hat{X}^+ = -i\omega\hat{a}$, simplifying the correlation function to the standard form.

A key observation in the USC regime is that in the eigenbasis of the Hamiltonian, the dressed light-matter jump operator \hat{X}^+ yields the correct expression for the ground state's excitation number: $\langle \phi_0 | \hat{X}^- \hat{X}^+ | \phi_0 \rangle = 0$, in contrast to the seemingly incorrect result $\langle \phi_0 | \hat{a}^\dagger \hat{a} | \phi_0 \rangle \neq$

0. The dressed ground state, expressed in the bare light-matter basis $\{|g\rangle, |e\rangle, |n\rangle\}$, contains virtual excitations [106]. To observe these as real photons, the coupling must be switched on and off, allowing the virtual excitations to be detected via the intracavity photon operator \hat{a} . This process, which should occur on the timescale of the system's relevant frequencies ω and Δ [106], allows the correct photon count $\langle \phi_k | \hat{a}^\dagger \hat{a} | \phi_k \rangle \neq 0$ to be obtained. The photons in the ground state are virtual and cannot be detected unless the coupling is abruptly switched off [25].

B. Quadrature Squeezing

The second-order correlation function, $G^{(2)}(0)$, often fails to serve as a reliable indicator of nonclassicality for a set of quantum states of light. Specifically, nonclassical Gaussian states, such as squeezed states, can display photon bunching or antibunching depending on the modulation of amplitude fluctuations. Therefore, to supplement $G^{(2)}(0)$ as a nonclassicality quantifier, we compute the degree of squeezing, which is more effective at revealing nonclassical behavior in these cases.

The degree of squeezing is computed by analyzing the generalized rotated field quadrature, defined as $\sqrt{2}\hat{x}_\theta = \hat{a}e^{-i\theta} + \hat{a}^\dagger e^{i\theta}$, where different values of θ correspond to distinct field quadratures. In particular, the quadratures $\hat{x}_{\theta=0}$ and $\hat{x}_{\theta=\pi/2}$ correspond to the position and momentum operators, respectively, which satisfy the commutation relations. The squeezing parameter is given by

$$\zeta^2 = \min_{\theta \in (0, 2\pi)} (\Delta \hat{x}_\theta)^2, \quad (23)$$

where the minimization is taken over all possible angles θ . A value of $\zeta^2 < 1$ indicates squeezing, while $\zeta^2 = 1$ corresponds to a coherent state.

Assuming the light-matter interaction has been switched off, the above expression simplifies to

$$\zeta^2 = 1 + 2\langle \hat{a}^\dagger \hat{a} \rangle - 2|\langle \hat{a}^2 \rangle|, \quad (24)$$

where the expectation values are taken considering the steady state.

It is worth noting that previous studies, such as Refs. [107, 108], have explored the squeezing of output quadratures in the USC and DSC regimes using dressed light-matter jump operators for a vacuum input field. Interestingly, these studies found that for any open system in its ground state, output squeezing cannot be produced, even if the ground state itself is squeezed. Since most of the squeezing in the two-qubit Rabi model is present in the ground state, this generalized measure leads to a zero degree of squeezing in the thermal state when the light-matter interaction is active. For this reason, we focus on evaluating the degree of squeezing after turning off the light-matter interaction. This process effectively transforms virtual photons into real, measurable

photons, revealing a clearer signature of squeezing in the system. Thus, after switching off the interaction, we capture the squeezing behavior by computing ζ^2 , highlighting the nonclassical features of the state.

C. Negativity

To investigate quantum correlations between the light-matter subsystems, we use the negativity $\mathcal{N}(\hat{\rho})$ as a measure of entanglement in bipartite systems [109–113]. The negativity is defined as

$$\mathcal{N}(\hat{\rho}) = \frac{\|\hat{\rho}^{TA}\|_1 - 1}{2}, \quad (25)$$

where $\hat{\rho}^{TA}$ is the partial transpose of the quantum state $\hat{\rho}$ with respect to subsystem A, and $\|\hat{Y}\|_1 = \text{Tr}|\hat{Y}| = \text{Tr}\sqrt{\hat{Y}^\dagger \hat{Y}}$ denotes the trace norm, or the sum of the singular values of the operator \hat{Y} . Alternatively, the negativity can be computed as $\mathcal{N}(\hat{\rho}) = \frac{1}{2} \sum_i (|\varepsilon_i| - \varepsilon_i)$, where ε_i are the eigenvalues of the partially transposed density matrix $\hat{\rho}$. A negativity of $\mathcal{N}(\hat{\rho}) = 0$ indicates that the state is separable, meaning it is not entangled.

D. Concurrence

The concurrence is a commonly used measure of entanglement for bipartite quantum systems. For a given two-qubit state $\hat{\rho}$, the concurrence is defined as

$$C(\hat{\rho}) = \max(0, \lambda_1 - \lambda_2 - \lambda_3 - \lambda_4), \quad (26)$$

where λ_i are the square roots of the eigenvalues of the matrix $\hat{\rho}\tilde{\rho}$, with $\tilde{\rho} = (\hat{\sigma}_y \otimes \hat{\sigma}_y)\hat{\rho}^*(\hat{\sigma}_y \otimes \hat{\sigma}_y)$, $\hat{\sigma}_y$ being the Pauli-Y matrix, and $\hat{\rho}^*$ is the matrix obtained by taking the complex conjugate of the elements of $\hat{\rho}$. The concurrence takes values between 0 and 1, with $C(\hat{\rho}) = 0$ indicating separable (non-entangled) states and $C(\hat{\rho}) = 1$ indicating maximally entangled states [114].

E. Mutual Information and Quantum Discord

Quantum discord (QD) is a measure of quantum correlations that goes beyond entanglement. It is based on the difference between two classically equivalent expressions for mutual information when applied to quantum systems. This expressions for a bipartite system \mathcal{AB} are defined as

$$\mathcal{I}(\hat{\rho}_{\mathcal{AB}}) = S(\hat{\rho}_A) + S(\hat{\rho}_B) - S(\hat{\rho}_{\mathcal{AB}}), \quad (27)$$

$$\mathcal{J}_A(\hat{\rho}_{\mathcal{AB}}) = S(\hat{\rho}_A) - S(\hat{\rho}_A|\hat{\rho}_B), \quad (28)$$

where $S(\hat{\rho}) = -\text{Tr}(\hat{\rho} \log_2 \hat{\rho})$ is the von Neumann entropy of the state $\hat{\rho}$, $S(\hat{\rho}_A)$ and $S(\hat{\rho}_B)$ are, respectively, the

entropies of the reduced density matrices of the subsystems A and B , and $S(\hat{\rho}_A|\hat{\rho}_B)$ is the conditional entropy of A given B . Quantum discord is then defined as the difference between these mutual informations, $\mathcal{D}(\hat{\rho}_{AB}) = \mathcal{I}(\hat{\rho}_{AB}) - \mathcal{J}_A(\hat{\rho}_{AB})$. Since $\mathcal{J}_A(\hat{\rho}_{AB})$ may take into account classical correlations, it must be maximized considering every possible set of projective measurements onto the eigenstates, in order to ensure the quantum discord computes only nonclassical correlations. This leads to

$$\mathcal{D}(\hat{\rho}_{AB}) = S(\hat{\rho}_A) - S(\hat{\rho}_{AB}) + \min_{\{\Pi_j^A\}} S(\hat{\rho}_{B|\{\Pi_j^A\}}), \quad (29)$$

where $S(\hat{\rho}_{B|\{\Pi_j^A\}})$ is the entropy conditioned by measurements on subsystem A . Quantum discord can be nonzero even for separable (non-entangled) states, distinguishing it from entanglement [115–117]. From now on, for the purposes of this work, when we cite mutual information, we will be referring to the definition of $\mathcal{I}(\hat{\rho}_{AB})$.

F. Quantum Coherence

Quantum coherence is a fundamental property of quantum systems and plays a crucial role in quantum information processing. It is typically characterized by the off-diagonal elements of the density matrix in a chosen basis. One prominent measure of quantum coherence is the coherence relative entropy, denoted here by C_{RE} , which quantifies the distance between a state $\hat{\rho}$ and its nearest diagonal (“classical”) state $\hat{\rho}_{\text{diag}}$. This is defined as

$$C_{\text{RE}} = S(\hat{\rho}_{\text{diag}}) - S(\hat{\rho}). \quad (30)$$

The coherence relative entropy provides a measure of the quantum coherence in a state, with $C_{\text{RE}} = 0$ indicating a diagonal (classical) state, and nonzero values signifying the presence of quantum coherence [2, 118].

It is important to emphasize that quantum coherence is basis-dependent. The coherence of a state can vary depending on the choice of measurement basis, meaning that different bases can reveal different aspects of the coherence. This basis-dependence is a key distinction between quantum coherence and classical correlations, the latter being invariant under changes in the measurement basis. Consequently, the measure of coherence on any given basis is not absolute but depends on the specific representation chosen for the system. In this study, we measure quantum coherence for the qubits in the S_z basis, where the off-diagonal elements of the density matrix are most indicative of coherence [2, 118].

G. Local Quantum Uncertainty

Local Quantum Uncertainty is a measure of the minimal quantum uncertainty achievable through a local measurement on a bipartite quantum system. It is based

on the skew information, which quantifies the deviation from commutativity between the quantum state and an observable. The skew information $\mathcal{K}(\hat{\rho}, \hat{K}_A)$ is defined as

$$\mathcal{K}(\hat{\rho}, \hat{K}_A) = -\frac{1}{2} \text{Tr}\{[\hat{\rho}^{\frac{1}{2}}, \hat{K}_A]^2\}, \quad (31)$$

where \hat{K}_A is the observable on subsystem A and $\hat{\rho}$ is the state of the bipartite system. This quantity is non-negative and vanishes if and only if the state and the observable commute, providing a natural measure of the quantum uncertainty due to noncommutativity [119].

The LQU is defined as the minimum skew information over all local observables in subsystem A of a bipartite system $\hat{\rho}_{AB}$, and is given by

$$\mathcal{U}_A(\hat{\rho}_{AB}) \equiv \min_{\hat{K}_A} \mathcal{I}(\hat{\rho}, \hat{K}_A). \quad (32)$$

For a system where both subsystems A and B are qubits, the minimization in Eq. (32) can be expressed in closed form, yielding a computable expression for $\mathcal{U}_A(\hat{\rho}_{AB})$. Specifically, for qubit-qubit systems, the LQU can be computed as

$$\mathcal{U}_A(\hat{\rho}_{AB}) = 1 - \lambda_{\max}\{W_{AB}\}, \quad (33)$$

where λ_{\max} is the maximum eigenvalue, and W_{AB} is a symmetric 3×3 matrix with elements

$$(W_{AB})_{ij} = \text{Tr}\left\{\hat{\rho}_{AB}^{1/2}(\hat{\sigma}_i^A \otimes \mathbb{I}_B)\hat{\rho}_{AB}^{1/2}(\hat{\sigma}_j^A \otimes \mathbb{I}_B)\right\},$$

where $\hat{\sigma}_i^A$ are the Pauli matrices ($i = x, y, z$) acting on subsystem A , and \mathbb{I}_B is the identity matrix acting on subsystem B .

For pure states $|\psi_{AB}\rangle$, this formula reduces to the linear entropy of entanglement

$$\mathcal{U}_A(\hat{\rho}_{AB}) = 2(1 - \text{Tr}(\hat{\rho}_A^2)),$$

where $\hat{\rho}_A$ is the reduced density matrix of subsystem A . In the case of maximally entangled pure states, the LQU is normalized to unity, reflecting maximal quantum uncertainty in the system [119].

IV. RESULTS AND DISCUSSION

We begin by examining the quantum properties associated with photon behavior, focusing on the second-order correlation function $G^{(2)}(0)$, which is calculated using the dressed jump operator. Fig. 2(a) illustrates its dependence on degenerate coupling strengths ($g_1 = g_2 = g$) and transition frequencies ($\Delta_1 = \Delta_2 = \Delta$) for a fixed mode frequency $\omega = 1$ and temperature $\mathbf{T} = 0.1$. Hereafter, we adopt natural units, expressing all parameters in terms of the lower frequency of the system. Specifically, we use the mode frequency in the high-frequency limit of the qubit and the qubit frequency in the regime of adiabatic quantum oscillators, as in Fig. 1.

Photon antibunching, characterized by $G^{(2)}(0) < 1$, emerges under specific spectral conditions in quantum systems governed by a general Hamiltonian. This phenomenon has been widely used to characterize the non-classicality of emitted photons [38–41]. Under thermal equilibrium, a critical requirement for achieving antibunching is the presence of a quasi-degenerate ground-state structure. In such cases, the ground state and the first excited state form a closely spaced doublet that is isolated from higher energy levels. This configuration ensures that, at low temperatures, thermal excitations remain confined primarily to these two states, minimizing the population in higher energy levels.

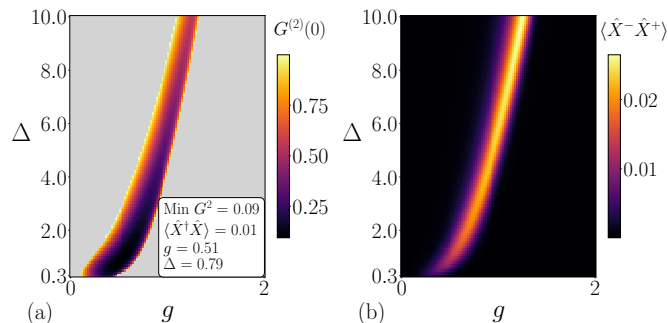


FIG. 2. Heatmaps of (a) the second-order correlation function $G^{(2)}(0)$ and (b) the number of excitations $\langle \hat{X}^- \hat{X}^+ \rangle$ as functions of the coupling strength g and the qubit frequency Δ for degenerate qubits ($\Delta_1 = \Delta_2 = \Delta$) and symmetric coupling ($g_1 = g_2 = g$) at a fixed temperature $\mathbf{T} = 0.1$, with $\omega = 1$. Regions with $G^{(2)}(0) \geq 1$ are shown in light gray in panel (a). The minimum value for the second-order correlation function, $G^{(2)}(0) = 0.09$, is observed at $g = 0.51$ and $\Delta = 0.79$, corresponding to excitation number of $\langle \hat{X}^- \hat{X}^+ \rangle = 0.01$.

Symmetry plays a pivotal role in constraining transitions within the system. For the eigenstates of the Hamiltonian of Eq. (1), the matrix elements $X_{jk} = \langle \phi_j | (\hat{a}^\dagger + \hat{a}) | \phi_k \rangle$ are restricted to transitions between states of differing parity. These symmetry constraints suppress multi-photon processes, thereby favoring single-photon emissions. Furthermore, the energy gap between the ground and first excited states (δ_{01}) must be significantly smaller than the gaps to higher levels ($\delta_{12}, \delta_{23}, \dots$). This energy hierarchy ensures that higher states remain thermally inaccessible or only weakly populated under typical low-temperature conditions, further reducing the likelihood of cascaded or multi-photon emissions. Nonlinearity in the spectrum also disrupts the resonance conditions that facilitate simultaneous multi-photon emissions, thereby favoring single-photon transitions [104, 105].

The interplay of these factors – quasi-degenerate states, symmetry constraints, and energy gap hierarchy – is evident in the two-qubit quantum Rabi model, particularly near resonance in the ultrastrong coupling regime. This behavior is depicted in Figs. 1(b) and corroborated in Fig. 2(a).

In Ref. [120], $G^{(2)}(0)$ was used to identify the breakdown of the rotating wave approximation far below the

conventional threshold of the ultrastrong coupling (USC) regime. The observed strong bunching behavior, characterized by $G^{(2)}(0) \gg 2$, was attributed to specific spectral features of the system. As shown in Fig. 2(a), regions where $G^{(2)}(0) > 1$ are highlighted in light gray, indicating that $G^{(2)}(0)$ cannot reliably serve as a nonclassicality quantifier in such cases, even when strong bunching occurs. Additionally, we note that antibunching-to-bunching transitions associated with first-order quantum phase transitions in the AQRM [64, 65] are absent here, consistent with observations in the standard QRM. It is worth noting that earlier studies on the thermal QRM and its variants predominantly focused on the resonant case. However, as demonstrated in Fig. 2, detuning offers two significant advantages. First, it facilitates the attainment of lower values of $G^{(2)}(0)$ at relatively small coupling strengths g , as seen in Fig. 2(a). Second, it enhances the photon emission rate from the resonator, which is proportional to $\langle \hat{X}^- \hat{X}^+ \rangle$ and detectable by a photon-absorber [106], as shown in Fig. 2(b). For the temperature under consideration, $\mathbf{T} = 0.1$, the minimum value of the equal-time second-order correlation function is $G^{(2)}(0) = 0.09$, occurring at a coupling strength of $g = 0.51$ and a qubit frequency of $\Delta = 0.79$, with a photon number $\langle \hat{X}^- \hat{X}^+ \rangle = 0.01$.

Beyond two-photon correlations, higher-order photon correlation functions have also been extensively studied to provide a more accurate characterization of photon statistics. These higher-order functions are closely related to phenomena such as multi-photon blockade and n -photon sources [121, 122]. However, for the given parameters at a temperature of $\mathbf{T} = 0.1$, the condition for two-photon blockade, i.e., $G^{(3)}(0) < 1$ and $G^{(2)}(0) > 1$, is not satisfied. As the information provided by the equal-time third-order correlation function, $G^{(3)}(0)$, is identical to that of $G^{(2)}(0)$ regarding the nonclassicality of the system, it has been omitted from the analysis.

The computation of $G^{(2)}(0)$ using the bare bosonic field, when the coupling strength is turned off after the system reaches thermal equilibrium, results in strong photon bunching up to the USC regime. As the light-matter coupling transitions into the DSC regime, $G^{(2)}(0)$ approaches unity, regardless of the detuning. This indicates statistical properties characteristic of a coherent state present in the thermal emission. In this scenario, the 2QQRM behaves identically to the QRM, and thus, the corresponding plots are omitted.

Fig. 3 shows the impact of temperature on the two-photon correlation function $G^{(2)}(0)$, presented in Fig. 3(a), and the number of excitations $\langle \hat{X}^- \hat{X}^+ \rangle$, depicted in Fig. 3(b), for various (symmetric) coupling strengths and (degenerate) qubit frequencies $\{g, \Delta\} = \{0.25, 1\}, \{0.5, 1\}, \{0.75, 1\}, \{0.5, 0.8\}, \{0.75, 2\}$. Notably, photon antibunching occurs only when $\mathbf{T} < 0.2$, and identical $G^{(2)}(0)$ values can be achieved for varying excitation numbers by carefully tuning the parameters $\{g, \Delta\}$.

To examine the degree of photonic squeezing, we

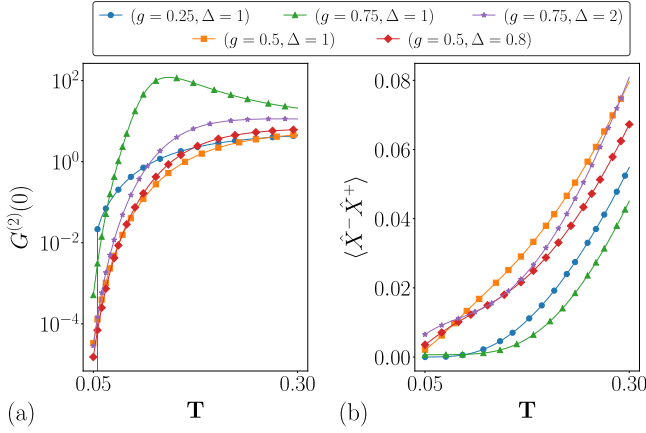


FIG. 3. (a) Temperature (\mathbf{T}) dependence of the second-order correlation function $G^{(2)}(0)$ and (b) the number of excitation $\langle \hat{X}^- \hat{X}^+ \rangle$ for a fixed mode frequency $\omega = 1$, with degenerate qubit frequencies $\Delta \in [0.8, 1, 2]$ and symmetric coupling strengths $g \in [0.25, 0.50, 0.75]$. For $\mathbf{T} < 0.1$, the second-order correlation function rapidly increases, while the number of excitations presents similar behavior for $\mathbf{T} > 0.1$.

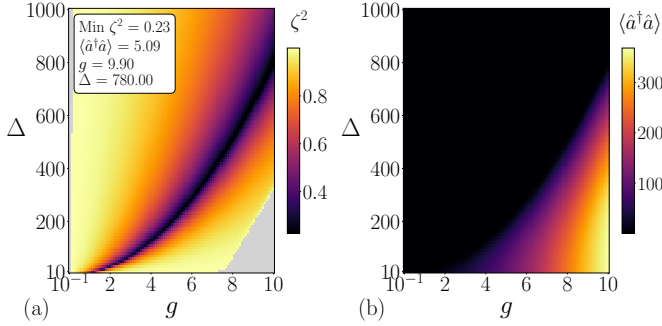


FIG. 4. Heatmaps of (a) the squeezing parameter ζ^2 and (b) the photon population $\langle \hat{a}^\dagger \hat{a} \rangle$ as functions of the symmetric coupling strength g and the degenerate qubit frequencies Δ , at a fixed temperature of $\mathbf{T} = 0.1$ and field frequency $\omega = 1$. In panel (a), regions where $\zeta^2 \geq 1$ are shown in light gray. The minimum squeezing parameter, $\zeta^2 = 0.23$, occurs at $g = 9.9$ and $\Delta = 780$, corresponding to a photon population of $\langle \hat{a}^\dagger \hat{a} \rangle = 5.09$. Strong squeezing is observed just below the critical coupling line $g_c = \sqrt{\omega\Delta}/2$, beyond which the system enters the superradiant phase, characterized by an increased photon population and a decrease in squeezing.

present heatmaps of the squeezing parameter ζ^2 in Fig. 4(a) and the photon population $\langle \hat{a}^\dagger \hat{a} \rangle$ in Fig. 4(b) as functions of symmetric coupling strengths $g_1 = g_2 = g$ and degenerate qubit frequencies $\Delta_1 = \Delta_2 = \Delta$, at a fixed temperature $\mathbf{T} = 0.1$ and mode frequency $\omega = 1$. In Fig. 4(a), regions with $\zeta^2 \geq 1$ are shown in light gray, while areas with $\zeta^2 < 1$ indicate significant photonic squeezing, occurring for specific coupling strengths within the range of the qubit frequencies. From the effective Hamiltonian of Eq. (15), squeezing is expected in the non-resonant regime. The minimum squeezing parameter, $\zeta^2 = 0.23$, is achieved at $g = 9.9$ and $\Delta = 780$, with a corresponding photon population of $\langle \hat{a}^\dagger \hat{a} \rangle = 5.09$. Ad-

ditionally, pronounced squeezing occurs just below the critical coupling strength $g_c = \frac{\sqrt{\omega\Delta}}{2}$, although the system does not strictly adhere to the thermodynamic limit $\omega/\Delta \rightarrow 0$. At these points, the system remains in the normal phase, which supports quadrature squeezing. In contrast, beyond g_c , the system transitions into the superradiant phase, characterized by high photon populations and the absence of squeezing, as illustrated in Fig. 4(b). For small g , squeezing increases with the coupling strength but remains weak near the qubit-photon resonance region. The strongest squeezing is observed in the high-frequency qubit regime, aligning with QRM ground-state results [38]. This behavior stems from the flattening of the oscillator's effective potential near the critical point, which leads to a significant enhancement in squeezing.

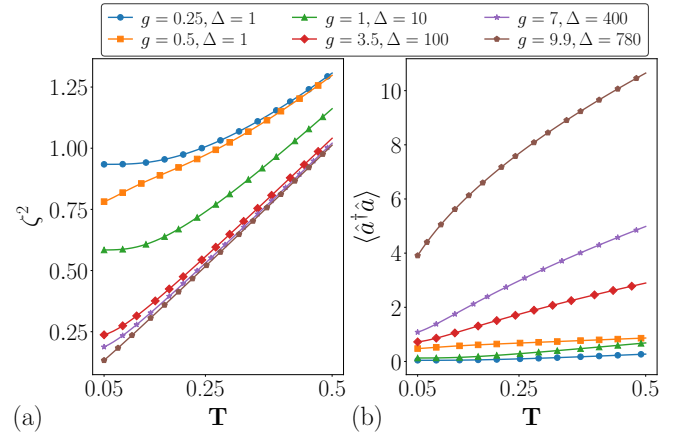


FIG. 5. Temperature (\mathbf{T}) dependence of the squeezing parameter ζ^2 (a) and photon population $\langle \hat{a}^\dagger \hat{a} \rangle$ (b) for a fixed mode frequency $\omega = 1$, with degenerate qubit frequencies $\Delta/\omega \in [1, 10, 100, 400, 780]$ and symmetric coupling strengths $g/\omega \in [1, 2, 3.5, 7, 9.9]$. For $\mathbf{T} < 0.1$, the squeezing parameter remains nearly constant while the photon population increases. As temperature rises, squeezing decreases linearly and vanishes around $\mathbf{T} \sim 0.5$, while the photon population continues to increase, especially at higher couplings.

In Fig. 5, we explore the impact of temperature on both the squeezing parameter ζ^2 and the photon population $\langle \hat{a}^\dagger \hat{a} \rangle$. Fig. 5(a) shows the squeezing parameter ζ^2 , and Fig. 5(b) displays the corresponding photon population as a function of temperature \mathbf{T} , expressed in units of the mode frequency ω . The analysis is performed for a fixed mode frequency $\omega = 1$, and a variety of qubit frequencies $\Delta_1 = \Delta_2 = \Delta \in [1, 10, 100, 400, 780]$, along with different coupling strengths $g_1 = g_2 = g \in [1, 2, 3.5, 7, 9.9]$. As observed in both panels of the figure, for low temperatures ($\mathbf{T} < 0.1$), the squeezing parameter remains nearly constant, as does the number of photons, indicating that the system continues to exhibit squeezing despite the presence of temperature. However, as the temperature increases, a noticeable change occurs: the squeezing decreases approximately linearly with temperature for all sets of qubit frequencies and coupling strengths.

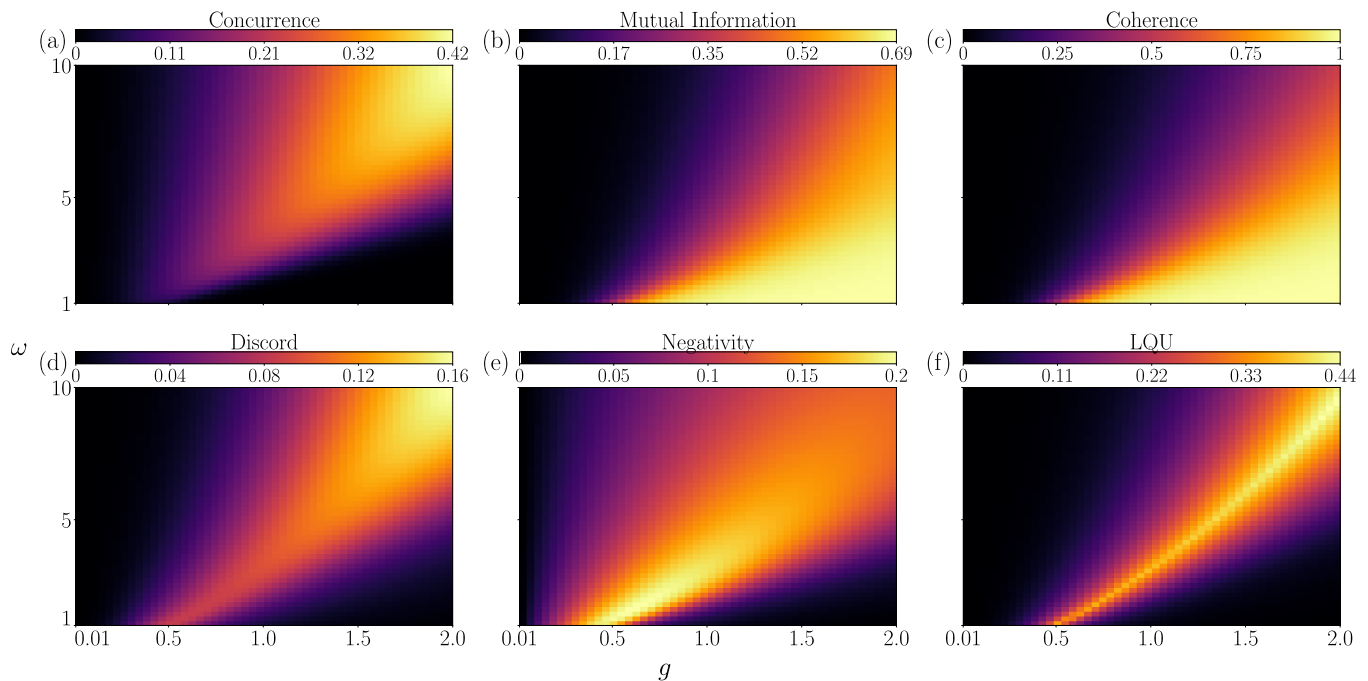


FIG. 6. Heatmaps showing nonclassicality quantifiers for the two qubits around resonance, as a function of the symmetric coupling strength g and the mode frequency ω , with a fixed temperature $\mathbf{T} = 0.1$. From top to bottom and left to right, the panels display (a) concurrence, (b) mutual information, (c) coherence, (d) quantum discord, (e) negativity, and (f) local quantum uncertainty (LQU). We set degenerate qubit frequencies $\Delta = 1$ in all plots.

This indicates how the thermal effects progressively reduce the degree of squeezing in the system. At temperatures around $\mathbf{T} \sim 0.5$, the system loses its ability to exhibit squeezing. Additionally, the photon population increases with temperature, especially at higher coupling strengths, reflecting the enhanced thermal excitation of the system. These results highlight the delicate balance between squeezing and thermal excitation, where squeezing is more robust at low temperatures and diminishes as thermal effects become more pronounced. Interestingly, squeezing survives to moderate temperatures, though it is reduced as the system is subjected to increased thermal energy. Furthermore, different couplings g_1 and g_2 and qubit frequencies Δ_1 and Δ_2 were studied, but no significant improvement was found in the achievable degree of squeezing, so these variations are omitted from the discussion.

We now examine the quantum correlations between the qubit-qubit, as well as between the field and the qubit. Fig. 6 presents heatmaps of these correlations around resonance as functions of the coupling strength g (ranging from 0 to 2) and the field transition frequency ω (ranging from 0.1 to 10) at a fixed temperature of $\mathbf{T} = 0.1$ and degenerate qubit frequencies $\Delta = 1$. Among the quantum correlation measures, negativity (Fig. 6(e)) is the weakest, remaining below $\mathcal{N}(\hat{\rho}_{\text{qubits}}) = 0.2$, even under optimal conditions where qubit and field frequencies are close in the USC regime. In contrast, other measures exhibit significant nonclassical signatures as the coupling strength increases and the system transitions into the

DSC regime. In this case, mutual information (Fig. 6(b)) and coherence (Fig. 6(c)) attain their highest values near resonance. Conversely, the best results for concurrence (Fig. 6(a)) and quantum discord (Fig. 6(d)) are found for large detunings. A similar behavior is observed for local quantum uncertainty (LQU, Fig. 6(f)), but it remains confined to a narrow range.

Notably, coherence reaches its theoretical upper bound ($C_{\text{RE}} = 1$), as expected from Eq. (21) in the adiabatic approximation. In this regime, the system's eigenstates are product states of displaced Fock states for the photons and x -polarized atomic states, $|\Phi\rangle = |j, m\rangle|\phi_m\rangle$, leading to vanishing qubit-photon entanglement. Mutual information is also substantial, approaching $\mathcal{I}(\hat{\rho}_{\text{qubits}}) \approx 0.7$, while concurrence and LQU reach moderate values, around $\mathcal{C}(\hat{\rho}_{\text{qubits}}) \sim \mathcal{U}(\hat{\rho}_{\text{qubits}}) \sim 0.4$. These results align with Ref. [87], which analyzed two ideal qubits interacting with a thermal-mechanical mode under resonance. However, our study extends this framework by exploring the impact of DSC at large detunings within a fully thermalized equilibrium state, a regime that has not been previously investigated.

Fig. 7 deepens our analysis by systematically exploring the effects of detuning over a broader parameter range. In non-resonant regimes, Eqs. (13) and (15) reveal the emergence of effective qubit-qubit interactions mediated by their dispersive coupling to the field. Specifically, Eq. (15) describes the non-RWA dispersive regime ($g \ll |\Delta - \omega|$), where strong quantum correlations are more favorably established. While coherence, Fig. 7(c),

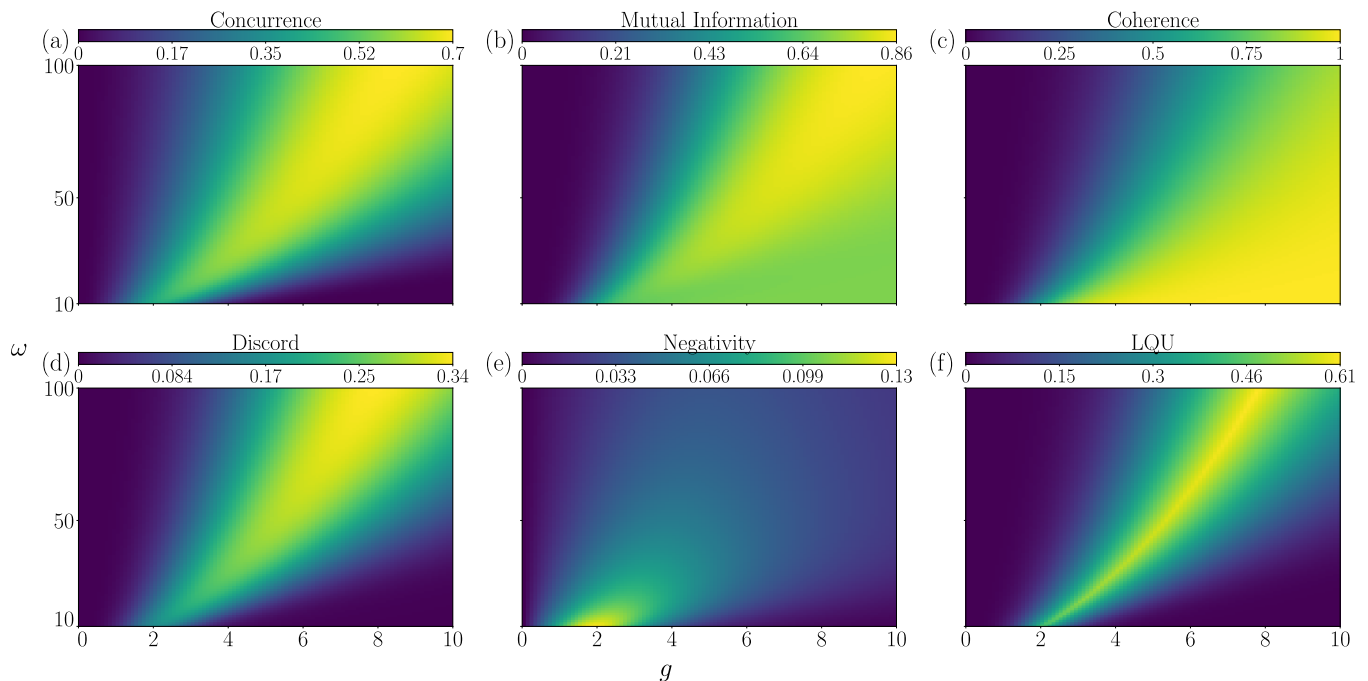


FIG. 7. Heatmaps displaying nonclassicality quantifiers for the two-qubit non-resonant scenario as functions of the symmetric coupling strength g and the field transition frequency ω , with a fixed temperature of $\mathbf{T} = 0.1$. The panels, arranged from top to bottom and left to right, show: (a) concurrence, (b) mutual information, (c) coherence, (d) quantum discord, (e) negativity, and (f) local quantum uncertainty (LQU). All plots assume degenerate qubit frequencies with $\Delta = 1$.

follows the same pattern observed previously, other correlation measures exhibit distinct changes. Most notably and also in agreement with the predictions from Eqs. (13) and (15), negativity (Fig. 7(e)) experiences a significant reduction – approximately halved – despite increasing the coupling strength up to $g = 10$. Conversely, larger detunings enhance the remaining quantum correlation quantifiers, with all optimal values occurring at higher field frequencies. Quantum discord, Fig. 7(d), exhibits the most pronounced improvement, more than doubling compared to Fig. 6(d), although it remains weaker than the other correlations, only surpassing negativity. Meanwhile, concurrence (Fig. 7(a)) and LQU (Fig. 7(f)) reach remarkable values, with $\mathcal{C}(\hat{\rho}_{\text{qubits}}) \sim 0.7$ and $\mathcal{U}(\hat{\rho}_{\text{qubits}}) \sim 0.6$, respectively. Mutual information, Fig. 7(b), also increases by approximately 10%, attaining $\mathcal{I}(\hat{\rho}_{\text{qubits}}) \approx 0.86$. These trends underscore the role of detuning in amplifying quantum correlations, particularly in the dispersive DSC regime.

To further enhance the nonclassical features of the two qubits and assess their robustness against parameter fluctuations, Fig. 8 qualitatively explores the effects of varying qubits' detunings on the most sensitive quantities, namely, concurrence (Figs. 8(a)-(d)), quantum discord (Figs. 8(b)-(e)), and local quantum uncertainty (Figs. 8(c)-(f)). Specifically, we fix the transition frequency of the first qubit at $\Delta_1 = 1$ and analyze two cases for the mode frequency: (i) $\omega = 10$ (top panels) and (ii) $\omega = 100$ (bottom panels). At first, it is worth noticing that the coupling strength g plays a decisive role in

the emergence of nonclassical effects, as these effects are suppressed in certain parameter regimes, specifically, at higher couplings in the top panels and at lower couplings in the bottom panels. In the top panels, where the field frequency is closer to the transition frequency of the first qubit, quantum correlations are enhanced at smaller values of g , allowing them to emerge even for varying Δ_2 . Conversely, in the bottom panels, when $\omega \gg \Delta_1$ (bottom panels), nonclassical effects strengthen with large coupling strength, $g > 4$.

Although the specific values of g influence the prominence of quantum correlations and their dependence on the second qubit's transition frequency, the maximum values occur for near-detuned qubits in both scenarios. Moreover, for a wide range of couplings, near-optimal results are achieved, highlighting the robustness of the system against parameter variations while preserving its quantum features.

In Fig. 9, we examine the impact of temperature on the nonclassical properties of the two qubits. From top to bottom and left to right, we present (a) concurrence, (b) mutual information (MI), (c) coherence, (d) quantum discord, (e) negativity, and (f) local quantum uncertainty (LQU) as functions of temperature \mathbf{T} . The analysis is performed for a fixed (degenerate) transition frequency $\Delta = 1$ of the qubits, considering a range of field frequencies $\omega \in [1, 10, 60, 100]$ and coupling strengths $g \in [0.25, 0.5, 1.0, 2.0, 6.0, 8.0]$.

Consistent with the observations in Fig. 5, the quantum properties of the qubits remain nearly constant at

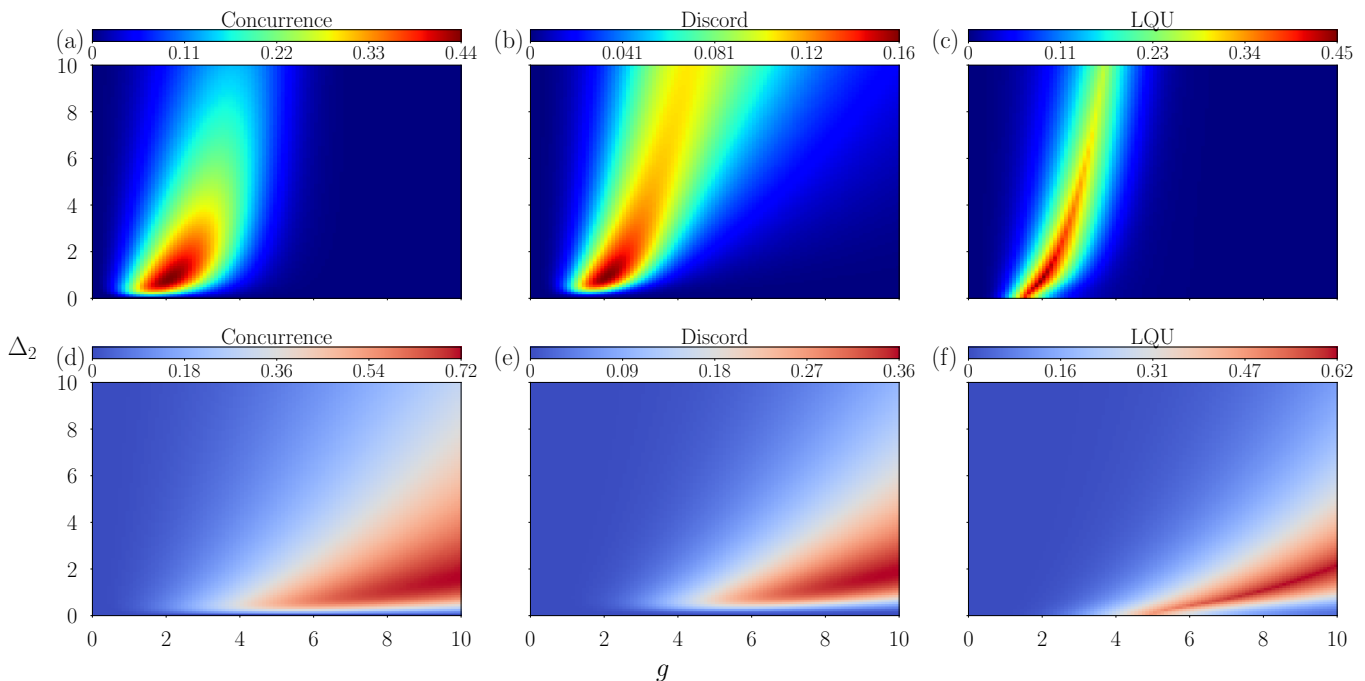


FIG. 8. Heatmaps showing the concurrence (a)-(d), quantum discord (b)-(e), and local quantum uncertainty (LQU) (c)-(f) as functions of the coupling strength g and the transition frequency Δ_2 of the second qubits. The field frequency is set to $\omega = 10$ in the top panels and $\omega = 100$ in the bottom panels. The temperature is held constant at $\mathbf{T} = 0.1$. In all cases, we set the frequency of the first qubit as $\Delta = 1$.

low temperatures ($\mathbf{T} \lesssim 0.1$), regardless of the chosen parameters. However, at higher temperatures, the behavior of different quantities diverges. Specifically, concurrence (Fig. 9(a)) and quantum discord (Fig. 9(c)) decay to zero, following a trend similar to the squeezing parameter and second-order correlation function. While negativity (Fig. 9(b)) and local quantum uncertainty (LQU, Fig. 9(d)) also decrease significantly, they remain measurable for certain parameter sets, even at $\mathbf{T} = 1$. In contrast, mutual information (Fig. 9(f)) generally vanishes rapidly with increasing temperature across most parameter configurations, with the exception of the resonant case where $g = \omega = 1$, where it survives up to $\mathbf{T} = 5$. Notably, at lower temperatures, some parameter sets (e.g., $g = \omega = 1$) yield nonzero mutual information while simultaneously exhibiting zero quantum discord, indicating that the correlations are predominantly classical in this regime. Conversely, parameter sets that produce both significant mutual information and quantum discord (e.g., $g = 6$ and $\omega = 60$) confirm the persistence of quantum correlations within the system. Lastly, coherence (Fig. 9(e)) initially increases with temperature before vanishing at higher \mathbf{T} , which is in agreement with recent studies [87]. This transient enhancement reveals a counterintuitive effect where thermal excitations temporarily amplify coherence, only for it to eventually degrade as the temperature continues to rise, thereby diminishing the system's quantum properties.

V. CONCLUDING REMARKS

In this study, we investigate the steady state of the 2QQRm by solving a dressed master equation at thermal equilibrium, which remains valid for arbitrary light-matter coupling strengths and yields a Gibbs state. Our key findings are as follows: (i) the emergence of quantum correlations and nonclassicality at thermal equilibrium. We show that quantum effects persist over a wide range of detunings and coupling strengths, even at moderate thermal temperatures, as confirmed by multiple measures of quantum correlation and nonclassicality; (ii) these quantum features are most prominent in the USC regime, particularly near the onset of the DSC regime and around criticality – where thermalization times may diverge – while they practically vanish in the deeper DSC regime; (iii) detuning plays a crucial role in enhancing nonclassicality and regulating the number of excitations. Furthermore, our results exhibit robustness across a broad parameter space without requiring fine-tuning of temperatures, frequencies, or coupling strengths.

The 2QQRm retains key nonclassical features of the QRM – particularly photon antibunching, though now peaking at half the characteristic coupling strength – while exhibiting several novel quantum behaviors. Although squeezing has been observed in the QRM in the high-frequency regime away from criticality at zero temperature [38] or under resonant conditions in thermal equilibrium [65], we demonstrate that the 2QQRm displays markedly different behavior: strong squeezing

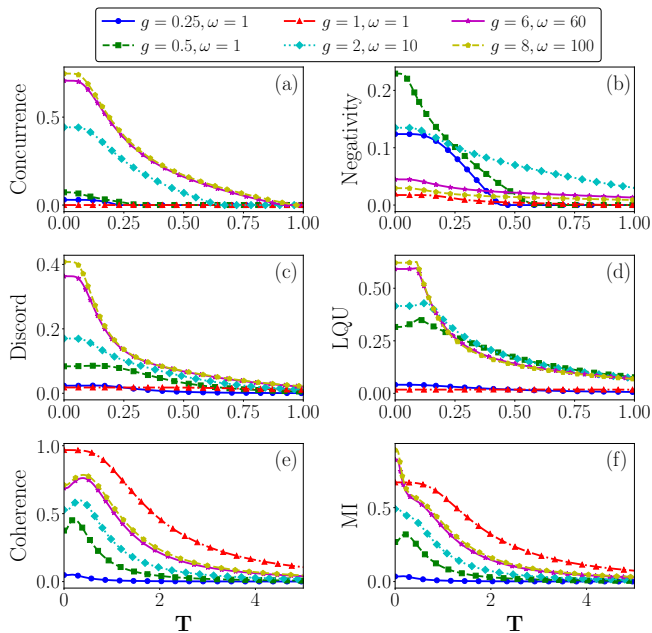


FIG. 9. Temperature (T) dependence of (a) concurrence, (b) negativity, (c) quantum discord, (d) local quantum uncertainty (LQU), (e) coherence, and (f) mutual information (MI) for a fixed qubit frequency $\Delta_1 = \Delta_2 = \Delta = 1$, with mode frequencies $\omega \in [1, 10, 60, 100]$ and coupling strengths $g \in [0.25, 0.5, 1.0, 2.0, 6.0, 8.0]$. For temperatures $T < 0.1$, all quantities remain nearly constant. As the temperature increases, for $T > 1.0$, only mutual information and coherence exhibit significant values.

emerges near criticality but becomes completely suppressed in the superradiant phase. Most importantly, we uncover three distinctive phenomena in the 2QQR that represent either qualitative departures from or entirely new features compared to the single-qubit case: (i)

diverging thermalization timescales; (ii) persistent entanglement between qubits (a feature fundamentally impossible in the single-qubit QRM); and (iii) robust quantum coherence with finite local quantum uncertainty – none of which have been systematically investigated for the QRM under thermal equilibrium conditions to date.

Our theoretical proposal to achieve nonclassical equilibrium states is both fundamentally significant and experimentally feasible, as recent advances in strong coupling and low-temperature techniques demonstrate. The USC regime, characterized by $g/\omega > 0.1$, has been experimentally realized for more than a decade [28] and continues to be realized in several systems [30]. The DSC regime, with $g/\omega \approx 1.34$ and a temperature of approximately 45 mK [31], is now within reach, with thermal entanglement observed in the quantum Rabi model. Deep-strong coupling considering the QRM is also observed with a single-trapped ion and, more recently, with trapped atoms [95], remarkably achieving couplings of ~ 6.5 greater than the field frequency [123]. Additionally, novel fluxonium-based superconducting devices are being developed to detect virtual photons in the USC regime [124]. Hybrid semiconductor-superconductor platforms further enhance flexibility in the implementation of the QRM [125], underscoring the exciting potential to realize nonclassical equilibrium states within these coupling regimes. Finally, USC is also reached using cold atoms [126] and metamaterials [127].

ACKNOWLEDGMENTS

This work was supported by the Coordenação de Aperfeiçoamento de Pessoal de Nível Superior - Brasil (CAPES) - Finance Code 001, National Council for Scientific and Technological Development (CNPq), Grant 311612/2021-0, and by the São Paulo Research Foundation (FAPESP), Grant 2022/00209-6 and Grant 2022/10218-2.

-
- [1] Eric Chitambar and Gilad Gour. Quantum resource theories. *Rev. Mod. Phys.*, 91:025001, Apr 2019.
 - [2] Alexander Streltsov, Gerardo Adesso, and Martin B. Plenio. Colloquium: Quantum coherence as a resource. *Rev. Mod. Phys.*, 89:041003, Oct 2017.
 - [3] Antonio Acín, Immanuel Bloch, Harry Buhrman, Tommaso Calarco, Christopher Eichler, Jens Eisert, Daniel Esteve, Nicolas Gisin, Steffen J Glaser, Fedor Jelezko, Stefan Kuhr, Maciej Lewenstein, Max F Riedel, Piet O Schmidt, Rob Thew, Andreas Wallraff, Ian Walmsley, and Frank K Wilhelm. The quantum technologies roadmap: a european community view. *New Journal of Physics*, 20(8):080201, aug 2018.
 - [4] Michael A. Nielsen and Isaac L. Chuang. *Quantum Computation and Quantum Information: 10th Anniversary Edition*. Cambridge University Press, 2010.
 - [5] Nicolas Gisin and Rob Thew. Quantum communication. *Nature Photonics*, 1(3):165–171, March 2007.
 - [6] Valerio Scarani, Helle Bechmann-Pasquinucci, Nicolas J. Cerf, Miloslav Dušek, Norbert Lütkenhaus, and Momtchil Peev. The security of practical quantum key distribution. *Rev. Mod. Phys.*, 81:1301–1350, Sep 2009.
 - [7] C. L. Degen, F. Reinhard, and P. Cappellaro. Quantum sensing. *Rev. Mod. Phys.*, 89:035002, Jul 2017.
 - [8] Vittorio Giovannetti, Seth Lloyd, and Lorenzo Maccone. Advances in quantum metrology. *Nature Photonics*, 5(4):222–229, March 2011.
 - [9] Vittorio Giovannetti, Seth Lloyd, and Lorenzo Maccone. Quantum metrology. *Phys. Rev. Lett.*, 96:010401, Jan 2006.
 - [10] Vittorio Giovannetti, Seth Lloyd, and Lorenzo Maccone. Quantum-enhanced measurements: Beating the standard quantum limit. *Science*, 306(5700):1330–1336, 2004.

- [11] Victor Montenegro, Marco G. Genoni, Abolfazl Bayat, and Matteo G. A. Paris. Quantum metrology with boundary time crystals. *Communications Physics*, 6(1):304, Oct 2023.
- [12] V. Montenegro, M. G. Genoni, A. Bayat, and M. G. A. Paris. Probing of nonlinear hybrid optomechanical systems via partial accessibility. *Phys. Rev. Res.*, 4:033036, Jul 2022.
- [13] V. Montenegro, M. G. Genoni, A. Bayat, and M. G. A. Paris. Mechanical oscillator thermometry in the nonlinear optomechanical regime. *Phys. Rev. Res.*, 2:043338, Dec 2020.
- [14] I. M. Georgescu, S. Ashhab, and Franco Nori. Quantum simulation. *Rev. Mod. Phys.*, 86:153–185, Mar 2014.
- [15] Wojciech Hubert Zurek. Decoherence, einselection, and the quantum origins of the classical. *Rev. Mod. Phys.*, 75:715–775, May 2003.
- [16] Kavan Modi, Aharon Brodutch, Hugo Cable, Tomasz Paterek, and Vlatko Vedral. The classical-quantum boundary for correlations: Discord and related measures. *Rev. Mod. Phys.*, 84:1655–1707, Nov 2012.
- [17] D. Mundarain and M. Orszag. Decoherence-free subspace and entanglement by interaction with a common squeezed bath. *Phys. Rev. A*, 75:040303, Apr 2007.
- [18] D. A. Lidar, I. L. Chuang, and K. B. Whaley. Decoherence-free subspaces for quantum computation. *Phys. Rev. Lett.*, 81:2594–2597, Sep 1998.
- [19] Daniel A. Lidar, David Bacon, Julia Kempe, and K. Birgitta Whaley. Protecting quantum information encoded in decoherence-free states against exchange errors. *Phys. Rev. A*, 61:052307, Apr 2000.
- [20] Lorenza Viola and Emanuel Knill. Random decoupling schemes for quantum dynamical control and error suppression. *Phys. Rev. Lett.*, 94:060502, Feb 2005.
- [21] L C Céleri, M A de Ponte, C J Villas-Boas, and M H Y Moussa. Switching off the reservoir through nonstationary quantum systems. *Journal of Physics B: Atomic, Molecular and Optical Physics*, 41(8):085504, apr 2008.
- [22] Florentin Reiter, David Reeb, and Anders S. Sørensen. Scalable dissipative preparation of many-body entanglement. *Phys. Rev. Lett.*, 117:040501, Jul 2016.
- [23] G. D. de Moraes Neto, V. F. Teizen, V. Montenegro, and E. Vernek. Steady many-body entanglements in dissipative systems. *Phys. Rev. A*, 96:062313, Dec 2017.
- [24] F. O. Prado, E. I. Duzzioni, M. H. Y. Moussa, N. G. de Almeida, and C. J. Villas-Bôas. Nonadiabatic coherent evolution of two-level systems under spontaneous decay. *Phys. Rev. Lett.*, 102:073008, Feb 2009.
- [25] G. D. de Moraes Neto, W. Rosado, F. O. Prado, and M. H. Y. Moussa. Steady entanglement in bosonic dissipative networks. *Phys. Rev. A*, 90:062322, Dec 2014.
- [26] Alexandre Blais, Steven M. Girvin, and William D. Oliver. Quantum information processing and quantum optics with circuit quantum electrodynamics. *Nature Physics*, 16(3):247–256, March 2020.
- [27] G. Wendin. Quantum information processing with superconducting circuits: a review. *Reports on Progress in Physics*, 80(10):106001, sep 2017.
- [28] Aji A. Anappara, Simone De Liberato, Alessandro Tredicucci, Cristiano Ciuti, Giorgio Biasiol, Lucia Sorba, and Fabio Beltram. Signatures of the ultrastrong light-matter coupling regime. *Phys. Rev. B*, 79:201303, May 2009.
- [29] T. Niemczyk, F. Deppe, H. Huebl, E. P. Menzel, F. Hocke, M. J. Schwarz, J. J. Garcia-Ripoll, D. Zueco, T. Hümmer, E. Solano, A. Marx, and R. Gross. Circuit quantum electrodynamics in the ultrastrong-coupling regime. *Nature Physics*, 6(10):772–776, July 2010.
- [30] P. Forn-Díaz, L. Lamata, E. Rico, J. Kono, and E. Solano. Ultrastrong coupling regimes of light-matter interaction. *Rev. Mod. Phys.*, 91:025005, Jun 2019.
- [31] Fumiki Yoshihara, Tomoko Fuse, Sahel Ashhab, Kosuke Kakuyanagi, Shiro Saito, and Kouichi Semba. Superconducting qubit-oscillator circuit beyond the ultrastrong-coupling regime. *Nature Physics*, 13(1):44–47, October 2016.
- [32] F. Yoshihara, T. Fuse, Z. Ao, S. Ashhab, K. Kakuyanagi, S. Saito, T. Aoki, K. Koshino, and K. Semba. Inversion of qubit energy levels in qubit-oscillator circuits in the deep-strong-coupling regime. *Phys. Rev. Lett.*, 120:183601, May 2018.
- [33] D. Meschede, H. Walther, and G. Müller. One-atom maser. *Phys. Rev. Lett.*, 54:551–554, Feb 1985.
- [34] R. J. Thompson, G. Rempe, and H. J. Kimble. Observation of normal-mode splitting for an atom in an optical cavity. *Phys. Rev. Lett.*, 68:1132–1135, Feb 1992.
- [35] C. Weisbuch, M. Nishioka, A. Ishikawa, and Y. Arakawa. Observation of the coupled exciton-photon mode splitting in a semiconductor quantum microcavity. *Phys. Rev. Lett.*, 69:3314–3317, Dec 1992.
- [36] Peter Lodahl, Sahand Mahmoodian, and Søren Stobbe. Interfacing single photons and single quantum dots with photonic nanostructures. *Rev. Mod. Phys.*, 87:347–400, May 2015.
- [37] Xiu Gu, Anton Frisk Kockum, Adam Miranowicz, Yu xi Liu, and Franco Nori. Microwave photonics with superconducting quantum circuits. *Physics Reports*, 718-719:1–102, 2017. Microwave photonics with superconducting quantum circuits.
- [38] S. Ashhab and Franco Nori. Qubit-oscillator systems in the ultrastrong-coupling regime and their potential for preparing nonclassical states. *Phys. Rev. A*, 81:042311, Apr 2010.
- [39] Li-Tuo Shen, Zhen-Biao Yang, Mei Lu, Rong-Xin Chen, and Huai-Zhi Wu. Ground state of the asymmetric rabi model in the ultrastrong coupling regime. *Applied Physics B*, 117(1):195–202, March 2014.
- [40] A. Ridolfo, S. Savasta, and M. J. Hartmann. Nonclassical radiation from thermal cavities in the ultrastrong coupling regime. *Phys. Rev. Lett.*, 110:163601, Apr 2013.
- [41] Luigi Garziano, Alessandro Ridolfo, Simone De Liberato, and Salvatore Savasta. Cavity qed in the ultrastrong coupling regime: Photon bunching from the emission of individual dressed qubits. *ACS Photonics*, 4(9):2345–2351, September 2017.
- [42] I. I. Rabi. On the process of space quantization. *Phys. Rev.*, 49:324–328, Feb 1936.
- [43] I. I. Rabi. Space quantization in a gyrating magnetic field. *Phys. Rev.*, 51:652–654, Apr 1937.
- [44] D. Braak. Integrability of the rabi model. *Phys. Rev. Lett.*, 107:100401, Aug 2011.
- [45] Daniel Braak, Qing-Hu Chen, Murray T Batchelor, and Enrique Solano. Semi-classical and quantum rabi models: in celebration of 80 years. *Journal of Physics A: Mathematical and Theoretical*, 49(30):300301, jun 2016.
- [46] Marlan O. Scully and M. Suhail Zubairy. *Quantum Optics*. Cambridge University Press, 1997.

- [47] Qing-Hu Chen, Yuan Yang, Tao Liu, and Ke-Lin Wang. Entanglement dynamics of two independent jaynes-cummings atoms without the rotating-wave approximation. *Phys. Rev. A*, 82:052306, Nov 2010.
- [48] Ferdi Altintas, Ali Ü. C. Hardal, and Özgür E. Müstecaplıoğlu. Rabi model as a quantum coherent heat engine: From quantum biology to superconducting circuits. *Phys. Rev. A*, 91:023816, Feb 2015.
- [49] G. Alvarado Barrios, F. Albarrán-Arriagada, F. A. Cárdenas-López, G. Romero, and J. C. Retamal. Role of quantum correlations in light-matter quantum heat engines. *Phys. Rev. A*, 96:052119, Nov 2017.
- [50] Gabriel Alvarado Barrios, Francisco J. Peña, Francisco Albarrán-Arriagada, Patricio Vargas, and Juan Carlos Retamal. Quantum mechanical engine for the quantum rabi model. *Entropy*, 20(10), 2018.
- [51] Yuan-Sheng Wang, Man-Hong Yung, Dazhi Xu, Maoxin Liu, and Xiaosong Chen. Critical behavior of the quantum stirling heat engine. *Phys. Rev. A*, 109:022208, Feb 2024.
- [52] He-Guang Xu, Jiasen Jin, Norton G. de Almeida, and G. D. de Moraes Neto. Exploring the role of criticality in the quantum otto cycle fueled by the anisotropic quantum rabi-stark model. *Phys. Rev. B*, 110:134318, Oct 2024.
- [53] S. Ashhab. Superradiance transition in a system with a single qubit and a single oscillator. *Phys. Rev. A*, 87:013826, Jan 2013.
- [54] Myung-Joong Hwang, Ricardo Puebla, and Martin B. Plenio. Quantum phase transition and universal dynamics in the rabi model. *Phys. Rev. Lett.*, 115:180404, Oct 2015.
- [55] Maoxin Liu, Stefano Chesi, Zu-Jian Ying, Xiaosong Chen, Hong-Gang Luo, and Hai-Qing Lin. Universal scaling and critical exponents of the anisotropic quantum rabi model. *Phys. Rev. Lett.*, 119:220601, Nov 2017.
- [56] Myung-Joong Hwang, M. S. Kim, and Mahn-Soo Choi. Recurrent delocalization and quasiequilibration of photons in coupled systems in circuit quantum electrodynamics. *Phys. Rev. Lett.*, 116:153601, Apr 2016.
- [57] Ricardo Puebla, Myung-Joong Hwang, and Martin B. Plenio. Excited-state quantum phase transition in the rabi model. *Phys. Rev. A*, 94:023835, Aug 2016.
- [58] Gaoke Hu, Wen-Long You, Maoxin Liu, and Haiqing Lin. Excited-state quantum phase transition in light-matter systems with discrete and continuous symmetries. *Phys. Rev. A*, 108:033710, Sep 2023.
- [59] Qiong-Tao Xie, Shuai Cui, Jun-Peng Cao, Luigi Amico, and Heng Fan. Anisotropic rabi model. *Phys. Rev. X*, 4:021046, Jun 2014.
- [60] Michael Tomka, Omar El Araby, Mikhail Pletyukhov, and Vladimir Gritsev. Exceptional and regular spectra of a generalized rabi model. *Phys. Rev. A*, 90:063839, Dec 2014.
- [61] E.T. Jaynes and F.W. Cummings. Comparison of quantum and semiclassical radiation theories with application to the beam maser. *Proceedings of the IEEE*, 51(1):89–109, 1963.
- [62] Li-Bao Fan, Yue-Hui Zhou, Fen Zou, Huan Guo, Jin-Feng Huang, and Jie-Qiao Liao. Quantum thermalization and vanishing thermal entanglement in the open jaynes-cummings model. *Annalen der Physik*, 532(8):2000134, 2020.
- [63] Wang-Yan Liu, Li-Bao Fan, Ye-Xiong Zeng, Jin-Feng Huang, and Jie-Qiao Liao. Quantum thermalization and thermal entanglement in the open quantum rabi model. *Annalen der Physik*, 535(2):2200502, 2023.
- [64] Tian Ye, Chen Wang, and Qing-Hu Chen. Implication of giant photon bunching on quantum phase transition in the dissipative anisotropic quantum rabi model. *Physica A: Statistical Mechanics and its Applications*, 609:128364, 2023.
- [65] He-Guang Xu, V. Montenegro, Gao Xianlong, Jiasen Jin, and G. D. de Moraes Neto. Persisting quantum effects in the anisotropic rabi model at thermal equilibrium. *Phys. Rev. Res.*, 6:013001, Jan 2024.
- [66] S A Chilingaryan and B M Rodríguez-Lara. The quantum rabi model for two qubits. *J. Phys. A: Math. Theor.*, 46:335301, 2013.
- [67] Jie Peng, Zhongzhou Ren, Daniel Braak, Guangjie Guo, Guoxing Ju, Xin Zhang, and Xiaoyong Guo. Solution of the two-qubit quantum rabi model and its exceptional eigenstates. *Journal of Physics A: Mathematical and Theoretical*, 47(26):265303, jun 2014.
- [68] Hui Wang, Shu He, Liwei Duan, Yang Zhao, and Qing-Hu Chen. Solutions to the quantum rabi model with two equivalent qubits. *Europhysics Letters*, 106(5):54001, may 2014.
- [69] Lijun Mao, Sainan Huai, and Yunbo Zhang. The two-qubit quantum rabi model: inhomogeneous coupling. *Journal of Physics A: Mathematical and Theoretical*, 48(34):345302, aug 2015.
- [70] Serge Haroche and Jean-Michel Raimond. *Exploring the Quantum: Atoms, Cavities, and Photons*. Oxford University Press, 08 2006.
- [71] T. Werlang, A. V. Dodonov, E. I. Duzzioni, and C. J. Villas-Bôas. Rabi model beyond the rotating-wave approximation: Generation of photons from vacuum through decoherence. *Phys. Rev. A*, 78:053805, Nov 2008.
- [72] T Grujic, S R Clark, D Jaksch, and D G Angelakis. Non-equilibrium many-body effects in driven nonlinear resonator arrays. *New Journal of Physics*, 14(10):103025, oct 2012.
- [73] G. Romero, I. Lizuain, V. S. Shumeiko, E. Solano, and F. S. Bergeret. Circuit quantum electrodynamics with a superconducting quantum point contact. *Phys. Rev. B*, 85:180506, May 2012.
- [74] Andrzej Janutka. Damping of multiphoton rabi oscillations and multiphoton purcell effect. *Journal of Physics A: Mathematical and General*, 39(3):577, dec 2005.
- [75] E. L. Raab, M. Prentiss, Alex Cable, Steven Chu, and D. E. Pritchard. Trapping of neutral sodium atoms with radiation pressure. *Phys. Rev. Lett.*, 59:2631–2634, Dec 1987.
- [76] J. M. Fink, R. Bianchetti, M. Baur, M. Göppl, L. Steffen, S. Filipp, P. J. Leek, A. Blais, and A. Wallraff. Dressed collective qubit states and the tavis-cummings model in circuit qed. *Phys. Rev. Lett.*, 103:083601, Aug 2009.
- [77] L. DiCarlo, J. M. Chow, J. M. Gambetta, Lev S. Bishop, B. R. Johnson, D. I. Schuster, J. Majer, A. Blais, L. Frunzio, S. M. Girvin, and R. J. Schoelkopf. Demonstration of two-qubit algorithms with a superconducting quantum processor. *Nature*, 460(7252):240–244, June 2009.
- [78] Stephan Welte, Bastian Hacker, Severin Daiss, Stephan Ritter, and Gerhard Rempe. Photon-mediated quantum

- gate between two neutral atoms in an optical cavity. *Phys. Rev. X*, 8:011018, Feb 2018.
- [79] M. Benito, J. R. Petta, and Guido Burkard. Optimized cavity-mediated dispersive two-qubit gates between spin qubits. *Phys. Rev. B*, 100:081412, Aug 2019.
- [80] Mika A. Sillanpää, Jae I. Park, and Raymond W. Simmonds. Coherent quantum state storage and transfer between two phase qubits via a resonant cavity. *Nature*, 449(7161):438–442, Sep 2007.
- [81] Jie Peng, Zhongzhou Ren, Guangjie Guo, and Guoxing Ju. Integrability and solvability of the simplified two-qubit rabi model. *J. Phys. A: Math. Theor.*, 45:365302, 2012.
- [82] Liwei Duan, Shu He, and Qing-Hu Chen. Concise analytic solutions to the quantum rabi model with two arbitrary qubits. *Annals of Physics*, 355:121–129, 2015.
- [83] Yu-Yu Zhang and Qing-Hu Chen. Generalized rotating-wave approximation for the two-qubit quantum rabi model. *Phys. Rev. A*, 91:013814, Jan 2015.
- [84] B M Rodríguez-Lara, S A Chilingaryan, and H M Moyacessa. Searching for structure beyond parity in the two-qubit dicke model. *Journal of Physics A: Mathematical and Theoretical*, 47(13):135306, Mar 2014.
- [85] Jie Peng, Juncong Zheng, Jing Yu, Pinghua Tang, G. Alvarado Barrios, Jianxin Zhong, Enrique Solano, F. Albarrán-Arriagada, and Lucas Lamata. One-photon solutions to the multiqubit multimode quantum rabi model for fast w -state generation. *Phys. Rev. Lett.*, 127:043604, Jul 2021.
- [86] Jie Peng, Jianing Tang, Pinghua Tang, Zhongzhou Ren, Junlong Tian, Nancy Barraza, Gabriel Alvarado Barrios, Lucas Lamata, Enrique Solano, and F. Albarrán-Arriagada. Deterministic single-photon source in the ultrastrong-coupling regime. *Phys. Rev. A*, 108:L031701, Sep 2023.
- [87] N Etehad Abari, A A Rakhubovsky, and R Filip. Correlated qubit coherences stimulated by thermal energy. *New Journal of Physics*, 26(8):083022, Aug 2024.
- [88] R. Grimaudo, G. Falci, A. Messina, E. Paladino, A. Sergi, E. Solano, and D. Valenti. Thermodynamic limit in the two-qubit quantum rabi model with spin-spin coupling. *Phys. Rev. Res.*, 6:043298, Dec 2024.
- [89] Thomas J. Hamlyn, Chi Zhang, Igor Lesanovsky, and Weibin Li. Tripartite quantum rabi model with trapped rydberg ions. *Phys. Rev. Res.*, 6:023223, May 2024.
- [90] Qing-Hu Chen, Chen Wang, Shu He, Tao Liu, and Ke-Lin Wang. Exact solvability of the quantum rabi model using bogoliubov operators. *Phys. Rev. A*, 86:023822, Aug 2012.
- [91] H. P. Breuer and F. Petruccione. *The theory of open quantum systems*. Oxford University Press, Great Clarendon Street, 2002.
- [92] David Zueco, Georg M. Reuther, Sigmund Kohler, and Peter Hänggi. Qubit-oscillator dynamics in the dispersive regime: Analytical theory beyond the rotating-wave approximation. *Phys. Rev. A*, 80:033846, Sep 2009.
- [93] S. Agarwal, S. M. Hashemi Rafsanjani, and J. H. Eberly. Tavis-cummings model beyond the rotating wave approximation: Quasidegenerate qubits. *Phys. Rev. A*, 85:043815, Apr 2012.
- [94] Jonas Larson and Elinor K Irish. Some remarks on ‘superradiant’ phase transitions in light-matter systems. *Journal of Physics A: Mathematical and Theoretical*, 50(17):174002, Mar 2017.
- [95] M.-L. Cai, Z.-D. Liu, W.-D. Zhao, Y.-K. Wu, Q.-X. Mei, Y. Jiang, L. He, X. Zhang, Z.-C. Zhou, and L.-M. Duan. Observation of a quantum phase transition in the quantum rabi model with a single trapped ion. *Nature Communications*, 12(1), Feb 2021.
- [96] Y. K. Wang and F. T. Hioe. Phase transition in the dicke model of superradiance. *Phys. Rev. A*, 7:831–836, Mar 1973.
- [97] He-Guang Xu, Jiasen Jin, G. D. M. Neto, and Norton G. de Almeida. Universal quantum otto heat machine based on the dicke model. *Phys. Rev. E*, 109:014122, Jan 2024.
- [98] Fabrizio Minganti, Alberto Biella, Nicola Bartolo, and Cristiano Ciuti. Spectral theory of liouvillians for dissipative phase transitions. *Phys. Rev. A*, 98:042118, Oct 2018.
- [99] Takashi Mori and Tatsuhiko Shirai. Symmetrized liouvillian gap in markovian open quantum systems. *Phys. Rev. Lett.*, 130:230404, Jun 2023.
- [100] Ye-Hong Chen, Zhi-Cheng Shi, Yu-Ran Zhang, Franco Nori, and Yan Xia. Suppressed energy relaxation in the quantum rabi model at the critical point. *arXiv preprint arXiv:2411.03710*, 2024.
- [101] J.R. Johansson, P.D. Nation, and Franco Nori. Qutip 2: A python framework for the dynamics of open quantum systems. *Computer Physics Communications*, 184(4):1234–1240, 2013.
- [102] Howard Carmichael. *Statistical methods in quantum optics 1: master equations and Fokker-Planck equations*, volume 1. Springer Science & Business Media, 1999.
- [103] Howard J Carmichael. *Statistical methods in quantum optics 2: Non-classical fields*. Springer Science & Business Media, 2009.
- [104] P. Rabl. Photon blockade effect in optomechanical systems. *Phys. Rev. Lett.*, 107:063601, Aug 2011.
- [105] A. Ridolfo, M. Leib, S. Savasta, and M. J. Hartmann. Photon blockade in the ultrastrong coupling regime. *Phys. Rev. Lett.*, 109:193602, Nov 2012.
- [106] L. Garziano, A. Ridolfo, R. Stassi, O. Di Stefano, and S. Savasta. Switching on and off of ultrastrong light-matter interaction: Photon statistics of quantum vacuum radiation. *Phys. Rev. A*, 88:063829, Dec 2013.
- [107] Roberto Stassi, Salvatore Savasta, Luigi Garziano, Bernardo Spagnolo, and Franco Nori. Output field-quadrature measurements and squeezing in ultrastrong cavity-qed. *New J. Phys.*, 18(12):123005, Dec 2016.
- [108] Changsuk Noh and Hyunchul Nha. Output field squeezing in a weakly-driven dissipative quantum rabi model. *Optics Communications*, 435:350–354, 2019.
- [109] Jens Eisert and Martin B. Plenio. A comparison of entanglement measures. *Journal of Modern Optics*, 46(1):145–154, 1999.
- [110] Karol Życzkowski, Paweł Horodecki, Anna Sanpera, and Maciej Lewenstein. Volume of the set of separable states. *Phys. Rev. A*, 58:883–892, Aug 1998.
- [111] M. B. Plenio. Logarithmic negativity: A full entanglement monotone that is not convex. *Phys. Rev. Lett.*, 95:090503, Aug 2005.
- [112] S. Lee, L. C. Kwek, and C. H. Oh. Partial transpose and negative eigenvalues of density matrices for two spin-1/2 systems. *Physical Review A*, 63(5):052305, 2000.
- [113] G. Vidal and R. F. Werner. Computable measure of entanglement. *Phys. Rev. A*, 65:032314, Feb 2002.

- [114] William K. Wootters. Entanglement of formation of an arbitrary state of two qubits. *Phys. Rev. Lett.*, 80:2245–2248, Mar 1998.
- [115] Shunlong Luo. Quantum discord for two-qubit systems. *Phys. Rev. A*, 77:042303, Apr 2008.
- [116] Raul Coto, Víctor Montenegro, Vitalie Eremeev, Douglas Mundarain, and Miguel Orszag. The power of a control qubit in weak measurements. *Scientific Reports*, 7(1), July 2017.
- [117] Mazhar Ali, A. R. P. Rau, and G. Alber. Quantum discord for two-qubit x states. *Phys. Rev. A*, 81:042105, Apr 2010.
- [118] T. Baumgratz, M. Cramer, and M. B. Plenio. Quantifying coherence. *Phys. Rev. Lett.*, 113:140401, Sep 2014.
- [119] Davide Girolami, Tommaso Tufarelli, and Gerardo Adesso. Characterizing nonclassical correlations via local quantum uncertainty. *Phys. Rev. Lett.*, 110:240402, Jun 2013.
- [120] Álvaro Nodar, Ruben Esteban, Unai Muniain, Michael J. Steel, Javier Aizpurua, and Mikołaj K. Schmidt. Identifying unbound strong bunching and the breakdown of the rotating wave approximation in the quantum rabi model. *Phys. Rev. Res.*, 5:043213, Dec 2023.
- [121] Eduardo Zubizarreta Casalengua, Juan Camilo López Carreño, Fabrice P. Laussy, and Elena del Valle. Conventional and unconventional photon statistics. *Laser & Photonics Reviews*, 14(6):1900279, 2020.
- [122] Christoph Hamsen, Karl Nicolas Tolazzi, Tatjana Wilk, and Gerhard Rempe. Two-photon blockade in an atom-driven cavity qed system. *Phys. Rev. Lett.*, 118:133604, Mar 2017.
- [123] Johannes Koch, Geram R. Hunanyan, Till Ockenfels, Enrique Rico, Enrique Solano, and Martin Weitz. Quantum rabi dynamics of trapped atoms far in the deep strong coupling regime. *Nature Communications*, 14(1):954, Feb 2023.
- [124] L. Giannelli, E. Paladino, M. Grajcar, G. S. Paroanu, and G. Falci. Detecting virtual photons in ultrastrongly coupled superconducting quantum circuits. *Phys. Rev. Res.*, 6:013008, Jan 2024.
- [125] D. J. van Woerkom, P. Scarlino, J. H. Ungerer, C. Müller, J. V. Koski, A. J. Landig, C. Reichl, W. Wegscheider, T. Ihn, K. Ensslin, and A. Wallraff. Microwave photon-mediated interactions between semiconductor qubits. *Phys. Rev. X*, 8:041018, Oct 2018.
- [126] A. Dareau, Y. Meng, P. Schneeweiss, and A. Rauschenbeutel. Observation of ultrastrong spin-motion coupling for cold atoms in optical microtraps. *Phys. Rev. Lett.*, 121:253603, Dec 2018.
- [127] Andreas Bayer, Marcel Pozimski, Simon Schambeck, Dieter Schuh, Rupert Huber, Dominique Bougeard, and Christoph Lange. Terahertz light-matter interaction beyond unity coupling strength. *Nano Letters*, 17(10):6340–6344, Oct 2017.